Research Square

Preprints are preliminary reports that have not undergone peer review.
They should not be considered conclusive, used to inform clinical practice,
or referenced by the media as validated information.

Neurogenesis ablation exacerbates dopaminergic dysfunction and fine motor deficits induced by 6-OHDA in rats

Bruna Araújo
i3S - Instituto de Investigação e Inovação em Saúde, Universidade do Porto
Rita Caridade-Silva
i3S - Instituto de Investigação e Inovação em Saúde, Universidade do Porto
Ana Vilaça-Ferreira
i3S - Instituto de Investigação e Inovação em Saúde, Universidade do Porto
Joana Martins-Macedo
i3S - Instituto de Investigação e Inovação em Saúde, Universidade do Porto
Catarina Teixeira
i3S - Instituto de Investigação e Inovação em Saúde, Universidade do Porto
Carla Soares-Guedes
i3S - Instituto de Investigação e Inovação em Saúde, Universidade do Porto
Teresa Summavielle
i3S - Instituto de Investigação e Inovação em Saúde, Universidade do Porto
Per Svenningsson
Department of Clinical Neuroscience, Karolinska Institutet
Luísa Pinto
Life and Health Sciences Research Institute (ICVS), School of Medicine, University of Minho
Fábio Gabriel Teixeira
fteixeira@i3s.up.pt

i3S - Instituto de Investigação e Inovação em Saúde, Universidade do Porto

Research Article

Keywords: Parkinson's Disease, Depression, Neurogenesis, Dopaminergic Degeneration

Posted Date: September 28th, 2026

DOI: https://doi.org/10.21203/rs.3.rs-10814574/v1

License: This work is licensed under a Creative Commons Attribution 4.0 International License.
Read Full License

Additional Declarations: No competing interests reported.

Abstract

Adult neurogenesis is increasingly recognised as a potential modulator of Parkinson's disease (PD) pathology, yet its interaction with dopaminergic degeneration remains poorly understood. Here, we investigated how ablation of adult neurogenesis influences dopaminergic vulnerability and associated motor outcomes using a combined rat model of conditional neurogenesis ablation (GFAP-Tk) and dopaminergic lesion (6-hydroxydopamine (6-OHDA)). Both neurogenesis suppression and dopaminergic lesions reduced hippocampal and subventricular zone (SVZ) proliferation. While dopaminergic lesion decreased Ki-67-positive cell density, it did not significantly alter neuroblast prevalence. In animals with impaired neurogenesis, tyrosine hydroxylase (TH) immunoreactivity was increased in the ventral hippocampus. In contrast, in the anterior amygdaloid area, only the combined manipulation reduced TH-positive fiber density, indicating region-specific monoaminergic adaptations. Further analyses of the SVZ revealed subregion-specific reduction in proliferation, with preservation of Ki67-positive cells in the lateral SVZ, suggesting potential shifts in progenitor fate and migration following injury. Importantly, these cellular alterations were accompanied by pronounced fine motor impairments in animals subjected to both neurogenesis ablation and dopaminergic lesion. Together, these findings indicate that reduced neurogenesis exacerbates dopaminergic dysfunction and associated motor deficits, highlighting a bidirectional interaction that may influence PD progression. Targeting this interplay may offer novel therapeutic targets to preserve neural plasticity and improve functional outcomes.

INTRODUCTION

Parkinson's disease (PD) is a progressive neurodegenerative disorder characterised primarily by the degeneration of dopaminergic neurons (DAn) in the substantia nigra pars compacta and the consequent depletion of dopamine within the nigrostriatal pathway(Marxreiter et al. 2013). Clinically, these neuropathological changes manifest as motor disturbances, including bradykinesia, rigidity, resting tremor, and postural instability, alongside a broad spectrum of non-motor symptoms, such as cognitive deficits, sleep disturbances, autonomic dysfunction, and mood disorders (Marxreiter et al. 2013). Depression is among the most prevalent and disabling non-motor symptoms of PD, affecting up to 40% of PD patients (Khedr et al. 2020; Prange et al. 2022). Unlike idiopathic major depressive disorder, depression in PD is closely linked to the underlying neurodegenerative processes. It may precede the onset of motor symptoms, appear at any stage of disease progression, and significantly worsen prognosis by reducing quality of life, accelerating cognitive decline, and complicating treatment responses (Jellinger 2022). Despite its clinical significance, the neurobiological basis of depression in PD remains incompletely understood, likely reflecting a complex interplay between neurotransmitter imbalance, neuroinflammation, and impaired neurogenesis (Zhao et al. 2025).

Although PD research has focused predominantly on nigrostriatal dysfunction, recent evidence supports a more widespread pattern of neurobiological disruption, involving limbic and hippocampal circuits that contribute to the complex phenotype of PD (Laakso et al. 1996; Camicioli et al. 2003). Reduced hippocampal neurogenesis has been associated with cognitive deficits, depression-like behaviors, and

altered stress responsiveness, conditions commonly observed in PD patients (Toda et al. 2019). In parallel, dopaminergic signalling has been reported to regulate neurogenic processes, with dopamine depletion leading to long-term alterations in progenitor proliferation and neuronal maturation (O'Keeffe et al. 2009; Garcia-Garrote et al. 2021). In fact, the hippocampus expresses key components of monoaminergic signalling, including enzymes and receptors involved in catecholamine synthesis and modulation, such as tyrosine hydroxylase (TH). Although TH is typically associated with dopaminergic and noradrenergic neurons, its presence in hippocampal interneurons and its afferent projections is well documented (Weihe et al. 2006; Tsetsenis et al. 2023). Altered TH expression within limbic structures has been observed in stress-related conditions, chronic inflammatory states, and transgenic models of dysrupted glial or neuronal function (McEwen et al. 2016). In PD, changes in hippocampal TH expression may reflect compensatory mechanisms, aberrant local catecholaminergic signalling, or structural remodelling following dopaminergic depletion (Kim et al. 2022, 2023; Wu and Liu 2024). Notably, TH dynamics specifically in the ventral hippocampus remain poorly explored, despite its prominent role in affective and stress-related behaviours that are frequently disrupted in early-stage PD (Hemmerle et al. 2012).

Despite growing recognition of the hippocampus as a significant locus of PD-related pathology, several questions remain unresolved. How does reduced adult neurogenesis interact with dopamine depletion to influence hippocampal-associated depressive symptoms? Do changes in TH expression represent compensatory mechanisms of maladaptive remodelling? Addressing these questions is essential for understanding the mechanisms underlying early depressive manifestations of PD, which often precede classical motor signs. To this end, this study investigated the combined effects of reduced adult hippocampal neurogenesis and dopaminergic degeneration using a dual-hit pre-clinical model – the transgenic GFAP- GFAP–thymidine kinase (GFAP-Tk) rat line subjected to 6-hydroxydopamine (6-OHDA)-induced dopaminergic lesions. In the GFAP-Tk model, the viral thymidine kinase (Tk) is expressed under the GFAP promoter. After administration of ganciclovir (GCV, a guanosine analog), proliferating cells incorporate the compound during DNA replication. The viral Tk metabolised the GFAP-positive proliferative cells, producing intracellular toxic products that ultimately induced cell death(Mateus-Pinheiro et al. 2021). By integrating behavioral, neurogenic, and dopaminergic analyses, this study provides insight into how suppression of hippocampal neurogenesis influences PD-related motor dysfunction and associated neural alterations.

MATERIAL AND METHODS

Stereotaxic surgeries and Ganciclovir treatment

All experiments were conducted with the consent of the Portuguese National Authority for Animal Care and Experimentation (Direção-Geral de Alimentação e Veterinária (DGAV), ID: DGAV005453), and in accordance with the local regulations on animal care and experimentation (European Union Directive 2010/63/ EU).

The GFAP-Tk transgenic Sprague-Dawley rats abrogated neurogenesis in the dentate gyrus and the subventricular zone of the olfactory bulbs. Cell-specific expression of the herpes simplex virus thymidine kinase (HSV-TK) enabled ablation of proliferating cells. The TK, but not the endogenous, phosphorylates analogues of nucleosides equivalent to ganciclovir, which was orally administered (Snyder et al. 2016). Those synthetic nucleosides are integrated into the DNA of cells during replication. This process allows for DNA synthesis to be inhibited, leading to apoptosis (Snyder et al. 2016). Additionally, this HSV-TK is controlled by the glial fibrillary acidic protein (GFAP) promoter, which promotes the reduction of newborn cells in the neurogenic brain regions: hippocampus and subventricular zone of the olfactory bulbs (Snyder et al. 2016). All the animals received ganciclovir (GCV, 50mg/Kg) for 21 consecutive days. GCV administration was omitted on days 7 and 14, which were designated as treatment off-days. Importantly, all animals were maintained under identical housing and environmental conditions throughout the study. The experimental design, sample size, and statistical analyses were established a priori before data collection. In addition to significance testing, effect size measures were calculated and reported to facilitate the interpretation of the results.

Prior to GCV administration, the PD model was induced using a protocol previously established by our group(Teixeira et al. 2017). Briefly, under the influence of ketamine-medetomidine (75 mg/kg; 0.5 mg/kg, intraperitoneally (i.p.)), 10-week-old male transgenic GFAP-Tk Sprague Dawley rats (n = 24) were unilaterally injected with 6-hydroxydopamine hydrochloride (6-OHDA) (2 µL at 4 µg/µL) combined with 0.2 mg/mL ascorbic acid in 0.9% NaCl; 6-OHDA group) directly into the striatum at specific coordinates related to Bregma and according to Paxinos and Watson brain atlas: AP: +1.3, ML: -2.6; AP: -1.3, ML: -4.5; AP: +0.4, ML: -3.0; AP: -0.4, ML: -4.2, DV: -5.0 (Paxinos and Watson 2007). The injection was administered at a rate of 1.0 µL/min using a 30-gauge needle and a Hamilton syringe (Hamilton, Bonaduz, CH, Switzerland) in a stereotaxic frame (Stoelting, Wood Dale, IL, USA). The vehicle groups received 2µL of 0.2 mg/mL ascorbic acid in 0.9% NaCl. In this experiment, the experimental groups included the wild-type animals (WT, n = 4), Tk animals (Tk, n = 4), WT animals with the 6-OHDA injections (WT 6-OHDA, n = 9), and Tk animals with 6-OHDA (Tk 6-OHDA, n = 8). Animals were randomly assigned to experimental groups before the study began.

Three weeks post-surgery, fine motor coordination was assessed. Upon completion of motor behaviour performance, rats were killed and processed for evaluation of dopaminergic neuron (DAn) loss and neurogenesis impairment by immunohistochemistry. During behavioural assessments, animals were not identified by visible markings that could reveal treatment allocation, thereby reducing observer-related bias. All in vivo experiments were conducted within a single experimental session, with animals from different experimental groups assessed in an interleaved manner. This approach prevented the consecutive evaluation of animals from the same treatment group and minimised potential order effects. Regarding the histological evaluations and cell quantification analyses, these were performed under blinded conditions, with investigators unaware of the treatment assignment of individual animals during data acquisition and analysis. Collectively, these procedures reduced experimental and analytical bias and enhanced the study's rigour, transparency, and reproducibility.

Staircase Behaviour Test

As reported in the literature, the loss of DAn caused by 6-OHDA unilateral administration, led to forelimb deficits in reaching, retrieving and eating the sugar pellets available in the staircase test (23,26). The staircase apparatus is composed of seven steps, which were classified as levels, in which level one is considered the easiest (closer to the animal) and level seven is the hardest one. One week before evaluations, the sugar pellets were placed in the home cage of the animals for them to get used to the flavour and smell. Then, each rat had two training sessions (one session per day) for 5 minutes on the first day, and 10 minutes on the second day. In these sessions, the animals (WT, n = 4; Tk, n = 4; WT 6-OHDA, n = 9; and Tk 6-OHDA, n = 8) were able to explore the apparatus. In the following seven days, the test session was conducted for 15 minutes. In the first 5 days of test sessions, the pellets were available on both sides of the apparatus, and in the last two days, the food was placed on one side – a forced-choice task. During all the test sessions, the animals did not get *ad libitum* food. The animals received 3 food pellets at the end of each test session for one week. The weight of the animals was controlled every two days. A humane end-point was considered 20% loss of the initial weight. The number of pellets dropped and eaten was quantified on the left and right sides. Also, the levels that the animals reached on day 5 were qualitatively analysed.

Apomorphine Turning Behaviour Test

Animals (WT, n = 4; Tk, n = 4; WT 6-OHDA, n = 9; and Tk 6-OHDA, n = 8) received a single subcutaneous injection of apomorphine hydrochloride (Sigma-Aldrich; 0.05 mg/kg) in the dorsum and, immediately after, were positioned on a rotameter apparatus (MED-RSS, Med Associates, Fairfax, VT) for 45 minutes (Teixeira et al. 2017, 2020). The number of rotations was recorded digitally, and the calculus of net contralateral rotations (difference between total ipsilateral and contralateral rotations) denoted the integrity of the dopaminergic system. Animals with higher ipsilateral rotations were associated with pronounced dopaminergic degeneration.

Histology Assessment

Approximately four weeks post-model induction, the animals were deeply anaesthetised with intraperitoneal injections of sodium pentobarbital (Eutasil 60 mg/kg; Ceva Santé Animale SA, Libourne, France). Transcardial perfusions were made using 0.9% NaCl and 4% paraformaldehyde (PFA; Merck & Co. Inc., Kenilworth, NJ, USA) dissolved in 0.01 M phosphate-buffered saline (PBS), followed by post-mortem tissue fixation for 48 hours in 4% PFA. Then, the tissue was placed in a 30% sucrose solution prepared in PBS 1X. Brains were placed in 3% agarose and collected in 40 µm sections using a vibratome (Leica Vibratome VT1000S; Leica Biosystems, Nußloch, Baden-Württemberg, Germany). The slices were collected into a 12-well plate and kept in PBS 1X with azide at 4ºC.

Immunofluorescence Staining

Four to five coronal sections of hippocampus, striatum (STR), substantia nigra (SN), subventricular zone (SVZ) and olfactory bulbs (OB) were selected to represent the rostro-caudal axis of the brain regions. The sections were immersed in heated citrate buffer (90ºC, pH 6.0) for 20 minutes. After equal the room temperature (RT), they were washed with PBS 1X and incubated with PBS-T 0.5% for 10 minutes. Blocking was carried out with 10% Normal Goat Serum (NGS) (Sigma-Aldrich, St. Louis, MO, USA) in PBS-T 0.5% for 1.5 hours, following an overnight incubation at 4ºC on an orbital shaker set to 60 rpm with the appropriate primary antibody combination diluted in PBS 1X and 3% NGS. As primary antibodies, we used: TH mouse (1:2000; Anti-tyrosine clone LNC1, Millipore, Cat# MAB318, Millipore, RRID:AB_2201528) or TH rabbit (1:2000; Anti-tyrosine Hydroxylase, Milipore, Cat# MAB152, Millipore, RRID:AB_2201528), DAT rabbit (1:200, Anti-dopamine transporter, Abcam, Cat# ab184451, Abcam, RRID: AB_2893263), Vmat2 rabbit (1:100; Anti-Vmat2, Abcam, Cat# ab259970, Abcam, RRID:AB_3099042); DCX mouse (1:100; Anti-doublecortin mouse, SC271390, Santa Cruz Biotechnology, RRID:AB_10610966), Ki67 rabbit (1:100; Anti-Ki67, Abcam, Cat# ab16667, Abcam, RRID:AB_302459). The specificity of the anti-tyrosine hydroxylase (TH) mouse antibody (Cat# MAB318) was previously validated by (Sen et al. 2019), who demonstrated specific labeling of catecholaminergic neuronal populations in the avian brain. The anti-tyrosine hydroxylase (TH) rabbit antibody (Cat# MAB152) was validated by (Mijatovic et al. 2007), including detection of TH expression associated with alterations in dopaminergic neurotransmission in a transgenic mouse model. The manufacturer validated the anti-dopamine transporter (DAT) rabbit antibody (Cat# ab184451) using anatomical negative controls (striatum versus lateral ventricle/liver) and immunoprecipitation experiments showing a single band at the expected molecular weight (around 69 kDa) (https://www.abcam.com/en-us/products/primary-antibodies/dopamine-transporter-antibody-epr19695-ab184451). Also, the manufacturer validated the anti-VMAT2 rabbit antibody (Cat# ab259970) through BOND RX™ validation procedures (https://www.abcam.com/en-us/products/primary-antibodies/vmat2-antibody-epr24197-51-ab259970). The specificity and reliability of the anti-doublecortin (DCX) mouse antibody (Cat# SC271390) and the anti-Ki67 rabbit antibody (Cat# ab16667) were comprehensively evaluated by (Ghibaudi et al. 2023), who assessed the consistency of DCX and Ki67 detection across multiple mammalian species and demonstrated robust and reproducible immunolabeling patterns.

The following day, after being washed with PBS 1X, the sections were incubated with secondary antibodies diluted in PBS 1X for 2 hours at RT on an orbital shaking platform set to 120 rpm (goat anti-mouse Alexa Fluor 488 (Cat# A-11029, RRID:AB_2534088), goat anti-rabbit Alexa Fluor 488 (Cat# A-11034, RRID:AB_2576217), and goat anti-rabbit Alexa Fluor 594 (Cat# A-11037, RRID:AB_2534095); all from Invitrogen/Thermo Fisher Scientific). The incubation with diamidino-2-phenylindole-dihydrochloride (1:1000, DAPI nuclear counterstain, Invitrogen / Thermo Fisher Scientific, Cat# D1306) followed the three washes with PBS 1X. Slices were mounted on superfrost® Plus slides (Cat# 631-0108P; VWR, Galdenaaksebaan, Leuven, Belgium) and covered with Permafluor (Epredia Lab Vision PermaFluor Aqueous Mounting Medium, Epredia, Cat# TA-030-FM). Autofluorescence controls were tested from sections that were not incubated with primary or secondary antibodies.

Immunofluorescence Image Acquisition

Distinct image acquisition workflows were established to scan the brain regions analysed. Firstly, we scanned the sections (4–5 sections/animal, WT, n = 2–3; Tk, n = 2–3; WT 6-OHDA, n = 8; and Tk 6-OHDA, n = 7) in a widefield microscope (Leica DMI6000 Timelapse, Leica Microsystems, Germany) with 10x magnification (HC PL FLUOTAR 10x/0.25 Ph1) to create an imaging map to observe DAPI and/or TH staining to facilitate the identification of lesioned and non-lesioned hemispheres. Images from both brain hemispheres were acquired for hippocampus, striatum, substantia nigra and olfactory bulb sections.

For the striatal regions, the 10x magnification objective acquired a mosaic image of the whole slice in its focal plane. For the other regions, a mosaic image was also constructed with a 20x or 40x magnification of the region of interest, but with different Z stacks. All the parameters used to capture the image are summarised in Supplementary Table 1.

Cell quantification and measurement of fluorescence intensity

For the assessment of dopaminergic degeneration, the dopaminergic neurons in the substantia nigra pars compacta (SNc), pars reticulata (SNr), and ventral tegmental area (VTA) were determined by counting the total number of TH+ cells normalised by the area (mm^2) analysed (4–5 sections/animal, WT, n = 2–3; Tk, n = 2–3; WT 6-OHDA, n = 8; and Tk 6-OHDA, n = 7). The same procedure was performed to quantify TH+ cells in the sub-regions of the OB. Additionally, DCX+ cells and Ki67 + cells were similarly quantified in the hippocampus, SVZ and OB. Manual counting of those cells was conducted using the multi-point tool from the Cell-Counter plugin in FIJI. The fluorescence intensity of TH, Vmat2 and DAT on the STR, as well as TH on the hippocampus, was determined considering the integrated density of the fluorescence staining normalised by the area considered (μm^2). The integrated density was assessed after a segmentation conducted through the LabKit tool of Fiji, in which a classifier was trained to identify specific staining in the slice. This segmentation generated areas corresponding to each pixel or group of pixels exhibiting staining in the slice. Then, we combined the output areas from segmentation with the areas of the brain regions studied. Thus, at the end, we obtained an integrated density of the areas that have staining within our region of interest. Therefore, a macro script was created for that purpose.

To delimit the areas of the regions studied in this work, we used two different Fiji plugins. The FASTMAP Fiji plugin allowed us to define SNc, SNr, and VTA in the midbrain; in the hippocampus, we could outline the dentate gyrus (DG), hilus, subgranular zone (SGZ), molecular layer and CA1-3; and in the OB: glomerular layer, outer plexiform layer, mitral layer, inner plexiform layer, granule layer, and subependymal zone. However, a slight adjustment in the areas for each section was performed with the polygon tool. The other tool was the ABBA Fiji plugin. This tool was mainly used on the striatum slices. After resizing the image to match the dimensions of the atlas images incorporated in ABBA, we obtained the areas for

striatal sections: dorsal striatum, fundus striatum, olfactory tubercle, anterior amygdalar area, cingulum bundle, globus pallidus external segment, and substantia innominata.

Also, a macro script was created to keep only the mentioned regions and delete all the others. In the case of SVZ, the lateral, dorsal and medial regions were drawn with the polygon tool since the Allen brain atlas, on which we based our analysis, did not contain those brain regions.

This region's identification was performed in both hemispheres, which we distinguish by the ipsilateral (lesion side) and contralateral side (non-lesioned side).

Statistical Analysis

The sample size of the present study was based on our previous work using the same 6-OHDA rat model of PD (Caridade-Silva et al. 2023). Considering this, an a priori sample size estimation was performed using a statistical power of 80%, a significance level (α) of 0.05, an estimated effect size of 0.3, and a standard deviation of 6.25. Based on the approach described by Kadam and Bhalerao (Bhalerao and Kadam 2010), the estimated sample size was approximately 6–7 animals per group, which is consistent with the group sizes used in the present work. As the primary objective of this study was to evaluate the impact of neurogenesis abrogation on PD progression, the experimental design focused primarily on the comparison between the WT 6-OHDA and GFAP-Tk 6-OHDA groups. Furthermore, the GFAP-Tk transgenic model is well established and extensively characterised in Dr. Luísa Pinto's Lab (Martins-Macedo et al. 2024). Therefore, in accordance with the principles of the 3Rs (Replacement, Reduction, and Refinement), we minimised the number of animals allocated to control groups while maintaining the ability to address the study objectives WT, n = 4; Tk, n = 4; WT 6-OHDA, n = 9; and Tk 6-OHDA, n = 8).

Statistical analysis was conducted using SPSS Statistics (version 28; IBM Co., Armonk, NY, USA) and GraphPad Prism 10 software for creating graphics (La Jolla, USA). The quantitative analyses were performed using measurements obtained from 4–5 anatomically matched sections per animal, spanning the anteroposterior axis of the region of interest. We adopted this approach to preserve biologically relevant regional information, as averaging values across sections could mask important differences between anterior and posterior subregions. The Shapiro-Wilk test assessed the normality assumption for all continuous variables by examining kurtosis measures and visualising normal histogram distributions. The identified outliers were removed from the analysis. Thus, for one-way ANOVA, Levene's test checked for homogeneity of variances, while Mauchly's test evaluated sphericity, both accepted when p-value ≥ 0.05, and Tukey's HSD was considered as a post-hoc test for all the analyses in which the four groups were compared. If the homogeneity of variances was not satisfied, we conducted a Welch ANOVA and Games-Howell post-hoc tests. In the case of normality not being met, we performed a Kruskal-Wallis non-parametric test. Thus, nonparametric statistical analyses were applied when the assumptions were not met.

The comparison between ipsi- and contralateral sides was statistically analysed using a two-tailed Student's t-test. If the data were not normally distributed, we ran a Mann-Whitney test. Lastly, in the

staircase test, a two-way ANOVA was performed using the same assumptions and settings as before.

All analyses were conducted with a 95% confidence interval, considering differences statistically significant when the p-value was ≤ 0.05. Appropriate effect sizes were computed for each test. Data is presented as mean values ± SD (standard deviation).

Lastly, investigators performed all experimental procedures, data collection, and statistical analyses while blinded to the experimental groups until analysis completion.

RESULTS

GFAP-Tk transgenic rats show suppression of adult neurogenesis

Reduced hippocampal neurogenesis is linked to molecular and behavioral alterations commonly seen in PD (Regensburger et al. 2014). Therefore, here we took advantage of the transgenic GFAP-rat model, that it is used to selectively ablate GFAP-expressing cells, especially proliferating astrocytes and neural stem/progenitor cells that express GFAP. This rat model is therefore useful for studying adult neurogenesis. Following ganciclovir treatment and 6-OHDA lesion (Fig. 1a,b), both GFAP-Tk (Tks) and 6-OHDA-injected animals exhibited a significant reduction in proliferating cells (Ki67+) within the dorsal and ventral subgranular zone (SGZ) of the hippocampus (dorsal SGZ: $X^2(3) = 11.120$, $p = 0.011$; $p_{WT/Tk} = 0.007$, $p_{WT/WT\ 6-OHDA} = 0.002$, $p_{WT/Tk\ 6-OHDA} = 0.018$; ventral SGZ: $X^2(3) = 9.583$, $p = 0.022$; $p_{WT/Tk} = 0.018$, $p_{WT/WT\ 6-OHDA} = 0.003$, $p_{WT/Tk\ 6-OHDA} = 0.04$)(Fig. 1c-e). Consistent with these findings, neuroblasts (DCX+) were significantly reduced in the dorsal SGZ in the TK groups (F_{Welch} (3, 35.353) = 31.668, $p < 0.001$, $\eta^2 = 0.431$)(Fig. 1f,h). In the ventral SGZ, a reduction in immature neurons was specifically observed in the Tk plus 6-OHDA group compared to 6-OHDA WT animals ($F_{(3,40)} = 3.029$, $p = 0.040$, $\eta^2 = 0.185$; Fig. 1g,h).

Given the anatomical proximity of the subventricular zone (SVZ) to the striatum, this neurogenic niche was further analysed across its lateral, medial and dorsal sub-regions (Fig. 2). As 6-OHDA lesions were applied unilaterally, hemispheric differences were also assessed. Across all groups, the ipsilateral hemisphere displayed significantly higher numbers of Ki67 + cells compared to the contralateral side (WT: $t(21) = -4.721$, $p < 0.001$, Cohen's d= -1.971; Tk: $U = 102$, $p = 0.027$; WT 6-OHDA: $U = 506.5$, $p < 0.001$; Tk 6-OHDA: $U = 289$, $p < 0.001$; Fig. 2a). However, hemisphere-dependent differences in immature neurons (DCX+) were only observed in the Tk 6-OHDA ($t_{(26)} = -2.548$, $p = 0.017$, Cohen's d= -0.963; Fig. 2b).

Due to these differences, subsequent analyses focused on the ipsilateral side. In the lateral SVZ, the density of Ki67 + cells was significantly reduced in the anterior region of the Tk 6-OHDA group compared to both WT and WT 6-OHDA animals ($F_{Welch(3,\ 12.675)} = 11.658$, $p < 0.001$, $\eta^2 = 0.151$; WT vs Tk 6-OHDA, p = 0.031, WT 6-OHDA vs Tk 6-OHDA, p = 0.006; Fig. 2d). In the medial SVZ, all experimental groups showed reduction of proliferative cells in comparison to WT animals ($X^2(3) = 12.683$, $p = 0.005$; $p_{WT/Tk}$<

0.001, $p_{WT/WT\ 6\text{-}OHDA}$= 0.024, $p_{WT/Tk\ 6\text{-}OHDA}$=0.006; Fig. 2g). Conversely, in the dorsal SVZ, reductions in Ki67 + cells were restricted to the posterior region in the Tk + 6-OHDA group ($X^2(3) = 12.026$, $p = 0.007$; $p_{WT\ 6\text{-}OHDA/Tk\ 6\text{-}OHDA}$= 0.003, $p_{Tk/Tk\ 6\text{-}OHDA}$= 0.015; Fig. 2k).

Analyses of DCX+ cells revealed that the lateral SVZ was the most affected subregion (Fig. 2m, u). Specifically, the Tk 6-OHDA group exhibited a significant reduction in the number in the posterior lateral SVZ ($X^2(3) = 9.438$, $p = 0.024$; $p_{WT\ 6\text{-}OHDA/Tk\ 6\text{-}OHDA}$= 0.047, $p_{WT/Tk\ 6\text{-}OHDA}$= 0.004; Fig. 2o). Qualitative distribution analyses supported these findings (Figs. 2v, 2x). In WT animals, Ki67 + cells were evenly distributed across SVZ subregions (Fig. 2v). However, in the Tk 6-OHDA group, 92% of proliferating cells were localised in the lateral SVZ (Fig. 2v). Similarly, while immature neurons in WT animals were predominantly located in the lateral SVZ, in the Tk 6-OHDA group, approximately half of DCX+ cells were found in the dorsal SVZ (Fig. 2x), indicating a shift in spatial distribution.

Given the involvement of the olfactory bulb (OB) in both PD and depression-related phenotypes (Regensburger et al. 2014), this region was also examined. No significant differences were observed in DCX+ cells (Supplementary Data 1). However, the number of TH+ cells in the OB's granule layer was increased in the Tk 6-OHDA group in comparison to WT 6-OHDA and Tk-induced groups ($X^2(3) = 8.395$, $p = 0.039$; Supplementary Data 2).

Disruption of neurogenesis amplifies 6-OHDA-driven dopaminergic degeneration beyond the nigrostriatal pathway

To determine whether neurogenesis suppression modulates dopaminergic vulnerability, we quantified dopaminergic neuron (DAn) densities across hemispheres (Fig. 3). Animals receiving 6-OHDA exhibited significant reductions in dopaminergic cell density in the ventral tegmental area (VTA) (Tk 6-OHDA: U = 196, $p = 0.010$; Fig. 3a), substantia nigra pars compacta (SNc) (WT 6-OHDA: U = 568, $p < 0.001$; Tk 6-OHDA: U = 310, $p < 0.001$; Fig. 3b) and substantia nigra pars reticulata (SNr) in the lesioned hemisphere (WT + 6-OHDA: U = 618, $p < 0.001$; Tk 6-OHDA: U = 299, $p < 0.001$; Fig. 3c). Given these hemisphere-specific effects, subsequent analyses focused on the ipsilateral (lesioned) side (Figs. 3d-f). 6-OHDA significantly reduced DAn cell densities in the 6-OHDA-injected animals compared to both the WT and Tk groups. Those DAn deficits were observed in VTA ($X^2(3) = 15.560$, $p = 0.001$; $p_{WT/WT\ 6\text{-}OHDA}$< 0.001, $p_{WT/Tk\ 6\text{-}OHDA}$=0.001, $p_{Tk/WT\ 6\text{-}OHDA}$=0.037, $p_{Tk/Tk\ 6\text{-}OHDA}$=0.036; Fig. 3d), SNc ($X^2(3) = 26.101$, $p < 0.001$; $p_{WT/WT\ 6\text{-}OHDA}$< 0.001, $p_{WT/Tk\ 6\text{-}OHDA}$<0.001, $p_{Tk/WT\ 6\text{-}OHDA}$<0.001, $p_{Tk/Tk\ 6\text{-}OHDA}$<0.001; Fig. 3e) and SNr ($X^2(3) = 13.411$, $p = 0.004$; $p_{WT/WT\ 6\text{-}OHDA}$=0.004, $p_{WT/Tk\ 6\text{-}OHDA}$=0.025, $p_{Tk/WT\ 6\text{-}OHDA}$=0.005, $p_{Tk/Tk\ 6\text{-}OHDA}$=0.041; Fig. 3f), indicating a pronounced disruption of dopaminergic system integrity.

Dopaminergic terminal integrity was assessed by measuring fluorescence intensity in the striatum (STR) and adjacent regions. A marked reduction in dopaminergic fibers was observed in the ipsilateral

caudoputamen of 6-OHDA-injected animals (WT: $t_{(20)}$=-0.695, p = 0.168, Cohen's d= -0.610; Tk: $t_{(18)}$=-0.467, p = 0.646, Cohen's d= -0.209; WT 6-OHDA: $t_{(60)}$=-14.997, p < 0.001, Cohen's d= -3.809; Tk 6-OHDA: $t_{(16)}$=-5.581, p < 0.001, Cohen's d= -2.647; Fig. 3h), whereas no significant hemispheric differences were detected in non-lesioned groups. Accordingly, analyses were restricted to the ipsilateral hemisphere.

Significant reductions in striatal DAn fibers were observed in 6-OHDA animals ($X^2(3)$ = 41.484, p < 0.001; $p_{WT/WT\ 6\text{-}OHDA}$< 0.001, $p_{WT/Tk\ 6\text{-}OHDA}$<0.001, $p_{Tk/WT\ 6\text{-}OHDA}$<0.001, $p_{Tk/Tk\ 6\text{-}OHDA}$<0.001; Fig. 3i), with consistent effects across both the anterior and posterior striatal regions (Anterior: $X^2(3)$ = 18.618, p < 0.001; $p_{WT/WT\ 6\text{-}OHDA}$< 0.001, $p_{WT/Tk\ 6\text{-}OHDA}$=0.006, $p_{Tk/WT\ 6\text{-}OHDA}$=0.003, $p_{Tk/Tk\ 6\text{-}OHDA}$=0.023; Fig. 3j; Posterior: $X^2(3)$ = 22.221, p < 0.001; $p_{WT/WT\ 6\text{-}OHDA}$< 0.001, $p_{WT/Tk\ 6\text{-}OHDA}$<0.001, $p_{Tk/WT\ 6\text{-}OHDA}$=0.003, $p_{Tk/Tk\ 6\text{-}OHDA}$=0.002; Fig. 3k).

Beyond the striatum, several regions exhibited significant reductions in TH fluorescence intensity following 6-OHDA lesion, including the fundus striatum (FS), olfactory tubercle (OT), substantia innominata (SI), globus pallidus external segment (GPe), anterior amygdalar area (AAA), and cingulum bundle (CB) (Figs. 3l-o). In general, both 6-OHDA groups showed reduced dopaminergic signal compared to WT animals (FS: $X^2(3)$ = 14.482, p = 0.002; $p_{WT/WT\ 6\text{-}OHDA}$< 0.001, $p_{WT/Tk\ 6\text{-}OHDA}$=0.003, Fig. 3l. OT: $F(3,27)$ = 4.019, p = 0.003, η^2 = 0.391; $p_{WT/WT\ 6\text{-}OHDA}$= 0.004, $p_{WT/Tk\ 6\text{-}OHDA}$=0.014, Fig. 3m. SI: $X^2(3)$ = 10.827, p = 0.013; $p_{WT/WT\ 6\text{-}OHDA}$= 0.002, $p_{WT/Tk\ 6\text{-}OHDA}$=0.029, Fig. 3n. GPe: $F(3,28)$ = 6.235, p = 0.002, η^2 = 0.400; $p_{WT/WT\ 6\text{-}OHDA}$= 0.010, $p_{WT/Tk\ 6\text{-}OHDA}$=0.039, Fig. 3o. AAA: $F(3,24)$ = 4.019, p = 0.019, η^2 = 0.334; $p_{WT/Tk\ 6\text{-}OHDA}$=0.027, Fig. 3p. CB: $X^2(3)$ = 8.107, p = 0.044; $p_{WT/WT\ 6\text{-}OHDA}$= 0.016, Fig. 3q). Tk animals showed a mild, non-significant reduction relative to WT, suggesting that neurogenesis ablation alone does not substantially impact dopaminergic tone in these regions. Region-specific effects emerged in the combined condition. In the GPe, WT 6-OHDA animals exhibited lower TH signal than Tk animals ($p_{Tk/WT\ 6\text{-}OHDA}$=0.03, Fig. 3o), whereas the Tk 6-OHDA group did not differ significantly, suggesting a potential modulatory effect of neurogenesis suppression. In contrast, in the AAA, the Tk 6-OHDA group showed reduced TH fluorescence intensity compared to Tk animals, indicating enhanced vulnerability in this region ($p_{Tk/Tk\ 6\text{-}OHDA}$=0.044, Fig. 3p).

Furthermore, analyses of dopamine transporter (DAT) fluorescence revealed a significant reduction in the ipsilateral hemisphere of 6-OHDA-injected animals (WT 6-OHDA: $t_{(34)}$=-5.865, p < 0.001, Cohen's d= -1.955; Tk 6-OHDA: $t_{(17)}$=-7.125, p < 0.001, Cohen's d= -3.274, Fig. 3r). Group comparisons confirmed an overall decrease in DAT signal in lesioned animals ($Fwelch_{(3,11.955)}$ = 12.368, $p < 0.001$, η^2 = 0.668; $p_{WT/WT\ 6\text{-}OHDA}$= 0.017, $p_{WT/Tk\ 6\text{-}OHDA}$=0.012, $p_{Tk/WT\ 6\text{-}OHDA}$= 0.034, $p_{Tk/Tk\ 6\text{-}OHDA}$=0.030, Fig. 3s).

In contrast, vesicular monoamine transporter 2 (Vmat2) expression as largely unchanged across groups (Fig. 4a-h). The only exception was the FS area, where WT animals exhibited higher Vmat2 fluorescence

intensity compared to all other groups ($X^2(3) = 14.148$, $p = 0.003$; $p_{WT/Tk} = 0.002$, $p_{WT/WT\ 6\text{–}OHDA} = 0.003$, $p_{WT/Tk\ 6\text{–}OHDA} = 0.017$, Fig. 4c).

Tyrosine hydroxylase levels are increased in the ventral hippocampus of 6-OHDA + GFAP-Tk animals

To evaluate the impact of DAn degeneration and reduced neurogenesis on hippocampal catecholaminergic signalling, TH fluorescence intensity was analysed across dorsal and ventral hippocampal subregions. No significant differences were detected in the dorsal hippocampal subregions, including DG (Fig. 5a), molecular layer (Fig. 5b), SGZ (Fig. 5c), hilus (Fig. 5d), CA1 (Fig. 5e), CA2 (Fig. 5f), and CA3 (Fig. 5g) across all experimental groups (Fig. 5a-h). However, increased TH fluorescence intensity was observed across most ventral subregions in groups with reduced neurogenesis (Fig. 5h-l, n), with the exception of the ventral CA2 region (Fig. 5m). In the ventral dentate gyrus (DG), Tk animals exhibited higher TH levels compared to both WT and WT 6-OHDA groups ($X^2(3) = 13.943$, $p = 0.003$; $p_{WT/Tk} = 0.048$, $p_{Tk/WT\ 6\text{–}OHDA} = 0.025$, Fig. 5h). Similarly, increased TH signal in Tk animals relative to WT 6-OHDA was observed in the molecular layer, SGZ, hilus, and CA1 (ventral molecular: $X^2(3) = 14.625$, $p = 0.002$; $p_{Tk/WT\ 6\text{–}OHDA} = 0.03$, Fig. 5i. ventral SGZ: $X^2(3) = 10.940$, $p = 0.012$; $p_{Tk/WT\ 6\text{–}OHDA} = 0.028$, Fig. 5j. ventral hilus: $FWelch_{(3,17.399)} = 31.668$, $p = 0.001$, $\eta^2 = 0.417$; $p_{Tk/WT\ 6\text{–}OHDA} = 0.022$, Fig. 5k. ventral CA1: $X^2(3) = 9.620$, $p = 0.022$; $p_{Tk/WT\ 6\text{–}OHDA} = 0.009$, Fig. 5l). The combined condition (Tk 6-OHDA) exhibited the most pronounced increases in TH fluorescence compared to both WT and WT 6-OHDA groups, TH levels were significantly elevated in the DG ($p_{WT/Tk\ 6\text{–}OHDA} = 0.012$; $p_{WT\ 6\text{–}OHDA/Tk\ 6\text{–}OHDA} = 0.002$, Fig. 5h), molecular layer ($p_{WT/Tk\ 6\text{–}OHDA} = 0.008$; $p_{WT\ 6\text{–}OHDA/Tk\ 6\text{–}OHDA} < 0.001$, Fig. 5i), SGZ ($p_{WT/Tk\ 6\text{–}OHDA} = 0.045$; $p_{WT\ 6\text{–}OHDA/Tk\ 6\text{–}OHDA} = 0.005$, Fig. 5j), hilus ($p_{WT/Tk\ 6\text{–}OHDA} = 0.010$; $p_{WT\ 6\text{–}OHDA/Tk\ 6\text{–}OHDA} = 0.003$, Fig. 5k). Within CA1 and CA3, differences were more restricted, with significant increases observed only relatively to WT 6-OHDA (CA1: $p_{WT\ 6\text{–}OHDA/Tk\ 6\text{–}OHDA} = 0.025$, Fig. 5l. CA3: $X^2(3) = 8.563$, $p = 0.036$; $p_{WT\ 6\text{–}OHDA/Tk\ 6\text{–}OHDA} = 0.018$, Fig. 5n).

Neurogenesis suppression exacerbates fine motor deficits in 6-OHDA-treated animals

To assess functional consequences of dopaminergic degeneration after 6-OHDA injections in the nigrostriatal pathway, motor performance was evaluated using the apomorphine-induced rotational test and the staircase task (17, 18). No significant differences were observed in apomorphine-induced rotations across groups ($X2(3) = 3.027$, $p = 0.387$; Fig. 6a), suggesting comparable levels of gross nigrostriatal asymmetry. In contrast, the staircase test revealed significant impairments in fine motor coordination. On the ipsilateral (left) side, both 6-OHDA-treated groups showed increased pellet dropping compared to WT animals, in which the most pronounced deficits observed in the Tk + 6-OHDA group (WT vs Tk 6-OHDA, $p < 0.001$; Tk vs Tk 6-OHDA, $p = 0.026$) (Fator time: $F_{(4,72)} = 2.794$, $p = 0.032$, $\eta2 = 0.134$;

Interaction between factors: $F_{(12,72)}$ = 1.439, p = 0.168, η2 = 0.193; Fator treatment: $F_{(12,72)}$) = 99.363, p < 0.001, η2 = 0.847; Fig. 6b). No significant differences were detected on the right contralateral side (Fig. 6c). Longitudinal analysis demonstrated that Tk 6-OHDA animals exhibited a progressive decline in motor performance, with a significant reduction in success rate (pellets retrieved and consumed) on the ipsilateral side over time (Fator time: $F_{(1.546,30.917)}$ = 17.392, p < 0.001, η2 = 0.465; Interaction between factors: $F_{(4.638,30.917)}$ = 3.269, p = 0.019, η2 = 0.329; Fator treatment: $F_{(1,20)}$ = 106.738, p < 0.001, η2 = 0.842; Fig. 6d). On the contralateral side, both WT and Tk animals outperformed compared to the Tk 6-OHDA group (Fator time: $F_{(1.803,36.057)}$ = 15.751, p < 0.001, η2 = 0.441; Interaction between factors: $F_{(5.409,36.057)}$ = 1.022, p = 0.422, η2 = 0.133; Fator treatment: $F_{(1,20)}$ = 78.012, p < 0.001, η2 = 0.796; Fig. 6e), indicating bilateral impairment in the combined condition (Fig. 6b-e).

Furthermore, analysis at the final testing day, when animals had reached performance plateau, confirmed these deficits. Lesioned animals showed reduced task proficiency compared to non-lesioned controls, reflected by increased pellet dropping and reduced pellet retrieval, particularly on the ipsilateral side (Fig. 6f-i). The non-lesioned animals reached higher difficulty-rate levels than those that received the neurotoxin (Fig. 6f, g). Regarding the pellets dropped on the left side, the 6-OHDA groups had more difficulty correctly retrieving the pellets than WT ($X^2(3)$ = 11.201, p = 0.011; $p_{WT/WT\ 6-OHDA}$=0.037, $p_{WT/Tk\ 6-OHDA}$=0.007, Fig. 6h). Additionally, the same differences were identified in the number of eaten pellets on the left and right sides (Left side: $X^2(3)$ = 15.442, p = 0.001; $p_{WT/WT\ 6-OHDA}$=0.003, $p_{WT/Tk\ 6-OHDA}$=0.002, Fig. 6h. Right side: $X^2(3)$ = 9.788, p = 0.02; $p_{WT/WT\ 6-OHDA}$=0.034, $p_{WT/Tk\ 6-OHDA}$=0.003, Fig. 6i), reinforcing their motor deficits induced by 6-OHDA. The 6-OHDA groups ate fewer sugar pellets than Tk animals on the left side ($p_{Tk/WT\ 6-OHDA}$=0.02, $p_{Tk/Tk\ 6-OHDA}$=0.011, Fig. 6h) and dropped less ($p_{Tk/Tk\ 6-OHDA}$=0.011, Fig. 6h). On the right side, they ate and dropped a similar number of pellets (Fig. 6i).

In the forced-choice condition, which isolates forelimb use, Tk 6-OHDA animals displayed severe impairments in reaching and consuming pellets on the ipsilateral side (Dropped: $X^2(3)$ = 8.370, p = 0.037; $p_{WT/Tk\ 6-OHDA}$=0.005, Fig. 6j. Eaten: $X^2(3)$ = 15.982, p = 0.001; $p_{WT/Tk\ 6-OHDA}$=0.006, $p_{Tk/Tk\ 6-OHDA}$<0.001, Fig. 6k). On the contralateral side, no significant differences were observed (Figs. 6j, k). In WT 6-OHDA animals, a lack of ability to retrieve sugar pellets on the ipsilateral side was also observed (Eaten: $p_{WT/WT\ 6-OHDA}$=0.043, $p_{Tk/WT\ 6-OHDA}$=0.006; Fig. 6k). Thus, these data suggest that a decrease in neurogenesis might impact the dopaminergic degeneration/function and motor performance.

Discussion

In this study, we investigated how suppression of adult neurogenesis influences dopaminergic neurodegeneration and associated motor outcomes. Our results demonstrate that combined adult neurogenesis ablation(Delaney et al. 1996; Snyder et al. 2016) and dopaminergic leosining produce region-specific alterations in monoaminergic signaling, accompanied by fine motor impairments. Consistent with previous studies, our experimental manipulations effectively reduced adult neurogenesis

and induced dopaminergic neuron loss. Additionally, it was not the scope of this work to focus on astrogliogenesis, but we cannot discard a potential effect of astrocytic proliferation. Notably, dopaminergic degeneration alone reduced the number of proliferative cells in the hippocampus, without significantly altering neuroblast prevalence (Suzuki et al. 2010). This dissociation suggests dopaminergic depletion may impair cell cycle progression rather than early neuronal differentiation. One possible mechanism involves the upregulation of cell cycle inhibitors such as $p27^{Kip1}$, which promotes cellular quiescence by regulating the G1 phase(Qiu et al. 2009; Patrício et al. 2013). Given the observed reduction in VTA dopaminergic neurons, and consequent decrease in hippocampal dopaminergic input, such mechanism may contribute to both the loss of newborn cells and the impaired maturation of progenitors at early stages of differentiation. These findings are consistent with the established role of dopamine in regulating hippocampal neurogenesis and neuronal maturation (Takamura et al. 2014; Kozareva et al. 2019; Ohira 2020).

A key finding of this study was the increase in TH immunoreactivity in the ventral hippocampus of animals with reduced neurogenesis (Tk and Tk 6-OHDA). This effect was absent in animals receiving 6-OHDA alone (WT 6-OHDA), indicating that neurogenesis suppression might underlie this phenotype (Fig. 5). Because TH labels both dopaminergic and noradrenergic neurons, this increase likely reflects compensatory catecholaminergic remodeling rather than simple dopaminergic preservation. One plausible mechanism involves noradrenergic projections from the locus coeruleus (LC), which densely innervate the hippocampus (Loughlin et al. 1986; Ermine et al. 2018), particularly the subgranular zone (Ermine et al. 2016), and are known to co-release norepinephrine and dopamine (Wu and Liu 2024). Importantly, LC neurons are relatively resistant to 6-OHDA-induced degeneration targeting midbrain dopaminergic neurons (Ermine et al. 2018). Additionally, TH labels catecholaminergic neurons broadly, including dopaminergic and noradrenergic neurons, because it detects the rate-limiting enzyme that converts L-tyrosine to L-DOPA (Weihe et al. 2006). Given that VTA and LC project to the dentate gyrus (DG), CA1, and CA3, and that SN pars compacta projects to CA2 (Yamasaki and Takeuchi 2017; Lai et al. 2024), our findings of increased TH staining in DG, hilus, CA1, and CA3 (but not CA2, which receives stronger substantia nigra input) point toward LC hyperinnervation as a compensatory response to dopaminergic loss and/or decreased hippocampal neurogenesis.

This interpretation is further supported by evidence linking noradrenergic activity to stress responses. Supporting this, Seki et al. described NA enhancement as a stress response (Seki et al. 2018), while stress is known to suppress neurogenesis and induce depressive- and anxiety-like behaviors(Herman 2010; Seki et al. 2018; Mateus-Pinheiro et al. 2021; Ribeiro et al. 2025). Sleep deprivation, a potent stressor, disrupts circadian rhythms and alters adult hippocampal neurogenesis(Mueller et al. 2013; Ali and von Gall 2022); its effects on neurogenesis depend on LC noradrenergic activity (Liu et al. 2024). Thus, the increased TH signal observed here may reflect a LC-mediated compensatory or stress-related response to reduced neurogenesis and altered network activity. The work by Seiriki et al., mapping LC projections further reinforces this interpretation, as they show that LC noradrenergic neurons strongly innervate ventral hippocampus, with dense axonal projections across hippocampal subregions (Seiriki et al. 2025). This aligns with our observation of enhanced TH labelling, particularly in the ventral

hippocampus. Given the role of the ventral hippocampus in emotional regulation and its connectivity with the amygdala, these changes may have functional relevance for affective symptoms associated with PD (Trivedi 2004). In line with this, we observed region-specific dopaminergic alterations in the anterior amygdaloid area (AAA), where only the combined condition (Tk 6-OHDA) resulted in reduced TH signal (Fig. 3). This suggests that neither neurogenesis suppression nor dopaminergic degeneration alone is sufficient to disrupt catecholaminergic innervation in this region (Fig. 3). The AAA is a key integrative hub receiving dopaminergic, noradrenergic(Fallon et al. 1978) and cholinergic inputs and is implicated in emotional processing and olfactory function(Gastard et al. 2002; Zheng et al. 2019). For instance, neuroimaging studies indicate AAA atrophy in Alzheimer's disease and major depression (Yao et al. 2020; Padulo et al. 2023), whereas AAA expansion occurs in PD(Zhang et al. 2024), highlighting its vulnerability to neurodegenerative processes. As a primary olfactory cortex structure receiving direct input from the olfactory bulb, the AAA participates in olfactory processing and projects reciprocally to olfactory regions(De Olmos et al. 2004). Given its reciprocal connectivity with both the hippocampus and olfactory bulb, dopaminergic and noradrenergic alterations in our model may, in turn, influence cholinergic circuits, potentially contributing to the TH changes observed in this region. Although LC provides noradrenergic projections to the amygdala(McCall et al. 2017), it remains unknown how reduced neurogenesis affects LC–amygdala connectivity. These findings raise the possibility that adult neurogenesis contributes to the stability of limbic monoaminergic circuits.

In contrast, we did not detect significant changes in dopaminergic cells in the olfactory bulb (OB), despite its documented involvement in early PD(Doty 2012) (Fig. 2). Findings in the literature vary, with studies reporting increased TH-positive OB neurons in PD patients(Huisman et al. 2004), while others report no changes(Cave et al. 2016). Additionally, patient-based imaging studies have shown that only the tremor-dominant PD subtype exhibits OB dysfunction, which correlates with striatal dopamine transporter loss (Nabizadeh et al. 2022). In contrast, animal models with bilateral 6-OHDA injections demonstrate increased TH-positive cells in the OB (Medeiros et al. 2024). However, our unilateral model may produce milder or delayed effects, as our data showed only a trend toward increased TH-positive densities in 6-OHDA-injected groups. Our results suggest that longer post-lesion intervals may be required to detect robust changes in this region.

Our analysis of the subventricular zone (SVZ) indicated region-specific reductions in cell proliferation after dopaminergic degeneration. The Tk + 6-OHDA group exhibited decreased Ki67-positive cells across SVZ subregions, with the anterior lateral, anterior medial, and posterior dorsal subregions particularly affected (Fig. 1). The observed alterations are consistent with known differences in neurogenic capacity and lineage output(Fiorelli et al. 2015; Chaker et al. 2016; Mizrak et al. 2019). Adult-born cells in the SVZ exist in quiescent, transitionary, or activated states(Chaker et al. 2016; Mizrak et al. 2019) and give rise to diverse neural populations, including neuroblasts, oligodendrocytes, astrocytes, granule cells(Fiorelli et al. 2015; Mizrak et al. 2019), and interneurons(Paul et al. 2017). In contrast, the spatial distribution and migration of newborn cells are regulated by region-specific physiological cues(Paul et al. 2017). For instance, the dorsal SVZ typically generates glutamatergic and GABAergic neurons and oligodendrocytes(Brill et al. 2009; Azim et al. 2016; Apostolou and Donega 2025), whereas the lateral

and medial regions primarily generate GABAergic neurons and oligodendrocytes(Brill et al. 2009; Azim et al. 2016; Apostolou and Donega 2025). In PD and 6-OHDA models, dopaminergic degeneration enhances GABAergic signalling in nigrostriatal pathways (Borgkvist et al. 2015). In fact, elevated GABA levels reduce SVZ proliferation and neuroblast production (Liu et al. 2005; Gascon et al. 2006)(Dittmann et al. 2025), and this may partially explain the global reduction in Ki67-positive cells observed in our study. Furthermore, anterior–posterior heterogeneity in neurogenic versus gliogenic output, established early in development(Luskin 1998), may underlie the observed region-specific reductions. Interestingly, in Tk + 6-OHDA animals, Ki67-positive cells were predominantly located in the lateral SVZ, which under physiological conditions gives rise to oligodendrocyte precursor cells(Alvarez-Buylla et al. 2020). Under injury conditions, SVZ-derived progenitors can alter their migration patterns and contribute to repair processes in adjacent regions such as the striatum(Alvarez-Buylla et al. 2020). Thus, despite an overall reduction in proliferation and neuroblast numbers (as indicated by Ki67- and DCX-positive cells), the SVZ appears to retain substantial plasticity in response to combined dopaminergic degeneration and impaired neurogenesis. Future studies should investigate the role of glial cells such as astrocytes (Privitera et al. 2024), and microglia, and and inflammatory signaling in shaping these responses.

Functionally, these cellular alterations were associated with significant impairments in fine motor performance. While apomorphine-induced rotations did not differ between groups, the staircase task revealed pronounced deficits in skilled forelimb use, particularly in animals with combined neurogenesis ablation and dopaminergic lesion. These impairments extended to both ipsilateral and contralateral limbs, suggesting deficits beyond classical unilateral motor dysfunction. Such effects may reflect disrupted integration of motor, motivational, and learning processes. Moreover, since most tests to assess depression-like behaviours in rodents are based on motor performance, these motor deficits precluded assessments of depression in this study (Wichmann et al. 2025). Dopaminergic neurons in the SN are essential for movement precision and action-specific learning execution, whereas those in the VTA contribute to motivation and reward-based learning(Fraser et al. 2023). The combined loss of these systems, together with impaired hippocampal plasticity, may underlie the observed behavioural deficits. Additionally, increased LC-mediated monoaminergic signalling may produce diffuse and less precise modulation, further impairing motor learning and performance.

Together, our results indicate that suppression of neurogenesis exacerbates dopaminergic dysfunction and contributes to both motor alterations. These results support a bidirectional interaction between neurogenesis and dopaminergic systems, with important implications for PD progression.

Finally, this work raises important questions regarding disease mechanisms. Does reduced neurogenesis precede and promote dopaminergic degeneration, or is it a downstream consequence of early dopaminergic dysfunction? Addressing this question will require longitudinal and circuit-level analyses. Understanding how impaired neurogenesis shapes network resilience may open new avenues for therapeutic intervention aimed at preserving neural plasticity and improving clinical outcomes in PD.

Declarations

Author Contribution

B.A. contributed to methodology, validation, formal analysis, investigation, writing of the original draft, and visualization. R.C.S. contributed to methodology, validation, investigation, and writing, review, and editing. A.V.F. contributed to methodology, validation, investigation, and writing, review, and editing. J.M.M. contributed to methodology, validation, investigation, and writing, review and editing. C.T. contributed to methodology, validation, and writing, review, and editing. C.S.G. contributed to methodology, validation, and writing, review and editing. T.S. contributed to writing, review and editing. P.S. contributed to writing, review and editing, and supervision. L.P. contributed to conceptualization, methodology, writing, review and editing, supervision, project administration, and funding acquisition. F.G.T. contributed to conceptualization, methodology, writing, review and editing, supervision, project administration, and funding acquisition. All authors read and approved the final manuscript.

Acknowledgement

We would like to thank Dr. Anderson Camargo for his critical reading of the manuscript.

Data Availability

The datasets supporting the findings of this study, including raw and processed behavioral and histological data obtained from the 6-OHDA GFAP-TK rat model, are available from the corresponding author upon reasonable request.

References

1. Ali AAH, von Gall C (2022) Adult Neurogenesis under Control of the Circadian System. Cells 11:764. https://doi.org/10.3390/cells11050764
2. Alvarez-Buylla A, Merkle FT, Fuentealba L, Cebrián-Silla A (2020) Neurogenesis in the postnatal V-SVZ and the origin of interneuron diversity. In: Patterning and Cell Type Specification in the Developing CNS and PNS. Elsevier, pp 505–522
3. Apostolou S, Donega V (2025) Embracing the heterogeneity of neural stem cells in the subventricular zone. Stem Cell Reports 20:102452. https://doi.org/10.1016/j.stemcr.2025.102452
4. Azim K, Berninger B, Raineteau O (2016) Mosaic Subventricular Origins of Forebrain Oligodendrogenesis. Front Neurosci 10:. https://doi.org/10.3389/fnins.2016.00107
5. Bhalerao S, Kadam P (2010) Sample size calculation. Int J Ayurveda Res 1:55. https://doi.org/10.4103/0974-7788.59946
6. Borgkvist A, Avegno EM, Wong MY, et al (2015) Loss of Striatonigral GABAergic Presynaptic Inhibition Enables Motor Sensitization in Parkinsonian Mice. Neuron 87:976–988. https://doi.org/10.1016/j.neuron.2015.08.022

7. Brill MS, Ninkovic J, Winpenny E, et al (2009) Adult generation of glutamatergic olfactory bulb interneurons. Nat Neurosci 12:1524–1533. https://doi.org/10.1038/nn.2416
8. Camicioli R, Moore MM, Kinney A, et al (2003) Parkinson's disease is associated with hippocampal atrophy. Movement Disorders 18:784–790. https://doi.org/10.1002/mds.10444
9. Caridade-Silva R, Araújo B, Martins-Macedo J, Teixeira FG (2023) N-Acetylcysteine Treatment May Compensate Motor Impairments through Dopaminergic Transmission Modulation in a Striatal 6-Hydroxydopamine Parkinson's Disease Rat Model. Antioxidants 12:1257. https://doi.org/10.3390/antiox12061257
10. Cave JW, Fujiwara N, Weibman AR, Baker H (2016) Cytoarchitectural changes in the olfactory bulb of Parkinson's disease patients. NPJ Parkinsons Dis 2:16011. https://doi.org/10.1038/npjparkd.2016.11
11. Chaker Z, Codega P, Doetsch F (2016) A mosaic world: puzzles revealed by adult neural stem cell heterogeneity. WIREs Developmental Biology 5:640–658. https://doi.org/10.1002/wdev.248
12. De Olmos JS, Beltramino CA, Alheid G (2004) Amygdala and Extended Amygdala of the Rat: A Cytoarchitectonical, Fibroarchitectonical, and Chemoarchitectonical Survey. In: The Rat Nervous System. Elsevier, pp 509–603
13. Delaney CL, Brenner M, Messing A (1996) Conditional Ablation of Cerebellar Astrocytes in Postnatal Transgenic Mice. The Journal of Neuroscience 16:6908–6918. https://doi.org/10.1523/JNEUROSCI.16-21-06908.1996
14. Dittmann NL, Chen L, Voronova A (2025) Regulation of neural stem cells by innervating neurons. J Neurochem 169:. https://doi.org/10.1111/jnc.16287
15. Doty RL (2012) Olfaction in Parkinson's disease and related disorders. Neurobiol Dis 46:527–552. https://doi.org/10.1016/j.nbd.2011.10.026
16. Ermine CM, Wright JL, Frausin S, et al (2018) Modelling the dopamine and noradrenergic cell loss that occurs in Parkinson's disease and the impact on hippocampal neurogenesis. Hippocampus 28:327–337. https://doi.org/10.1002/hipo.22835
17. Ermine CM, Wright JL, Parish CL, et al (2016) Combined immunohistochemical and retrograde tracing reveals little evidence of innervation of the rat dentate gyrus by midbrain dopamine neurons. Front Biol (Beijing) 11:246–255. https://doi.org/10.1007/s11515-016-1404-4
18. Fallon JH, Koziell DA, Moore RY (1978) Catecholamine innervation of the basal forebrain II. Amygdala, suprarhinal cortex and entorhinal cortex. Journal of Comparative Neurology 180:509–531. https://doi.org/10.1002/cne.901800308
19. Fiorelli R, Azim K, Fischer B, Raineteau O (2015) Adding a spatial dimension to postnatal ventricular-subventricular zone neurogenesis. Development 142:2109–2120. https://doi.org/10.1242/dev.119966
20. Fraser KM, Pribut HJ, Janak PH, Keiflin R (2023) From Prediction to Action: Dissociable Roles of Ventral Tegmental Area and Substantia Nigra Dopamine Neurons in Instrumental Reinforcement. The Journal of Neuroscience 43:3895–3908. https://doi.org/10.1523/JNEUROSCI.0028-23.2023

21. Garcia-Garrote M, Parga JA, Labandeira PJ, et al (2021) Dopamine Regulates Adult Neurogenesis in the Ventricular-Subventricular Zone via Dopamine < scp>D3</scp> Angiotensin Type 2 Receptor Interactions. Stem Cells 39:1778–1794. https://doi.org/10.1002/stem.3457
22. Gascon E, Dayer AG, Sauvain M-O, et al (2006) GABA Regulates Dendritic Growth by Stabilizing Lamellipodia in Newly Generated Interneurons of the Olfactory Bulb. The Journal of Neuroscience 26:12956–12966. https://doi.org/10.1523/JNEUROSCI.4508-06.2006
23. Gastard M, Jensen SL, Martin III JR, et al (2002) The caudal sublenticular region/anterior amygdaloid area is the only part of the rat forebrain and mesopontine tegmentum occupied by magnocellular cholinergic neurons that receives outputs from the central division of extended amygdala. Brain Res 957:207–222. https://doi.org/10.1016/S0006-8993(02)03513-8
24. Ghibaudi M, Amenta A, Agosti M, et al (2023) Consistency and Variation in Doublecortin and Ki67 Antigen Detection in the Brain Tissue of Different Mammals, including Humans. Int J Mol Sci 24:2514. https://doi.org/10.3390/ijms24032514
25. Hemmerle AM, Herman JP, Seroogy KB (2012) Stress, depression and Parkinson's disease. Exp Neurol 233:79–86. https://doi.org/10.1016/j.expneurol.2011.09.035
26. Herman JP (2010) Regulation of the HPA Axis by Acute and Chronic Stress. In: Encyclopedia of Behavioral Neuroscience. Elsevier, pp 149–153
27. Huisman E, Uylings HBM, Hoogland P V. (2004) A 100% increase of dopaminergic cells in the olfactory bulb may explain hyposmia in Parkinson's disease. Movement Disorders 19:687–692. https://doi.org/10.1002/mds.10713
28. Jellinger KA (2022) The pathobiological basis of depression in Parkinson disease: challenges and outlooks. J Neural Transm 129:1397–1418. https://doi.org/10.1007/s00702-022-02559-5
29. Khedr EM, Abdelrahman AA, Elserogy Y, et al (2020) Depression and anxiety among patients with Parkinson's disease: frequency, risk factors, and impact on quality of life. Egypt J Neurol Psychiatr Neurosurg 56:116. https://doi.org/10.1186/s41983-020-00253-5
30. Kim B, Kim J-S, Youn B, Moon C (2023) Dopamine depletion alters neuroplasticity-related signaling in the rat hippocampus. Anim Cells Syst (Seoul) 27:436–446. https://doi.org/10.1080/19768354.2023.2294308
31. Kim B, Weerasinghe-Mudiyanselage PDE, Ang MJ, et al (2022) Changes in the Neuronal Architecture of the Hippocampus in a 6-Hydroxydopamine-Lesioned Rat Model of Parkinson Disease. Int Neurourol J 26:S94-105. https://doi.org/10.5213/inj.2244252.126
32. Kozareva DA, Cryan JF, Nolan YM (2019) Born this way: Hippocampal neurogenesis across the lifespan. Aging Cell 18:. https://doi.org/10.1111/acel.13007
33. Laakso MP, Partanen K, Riekkinen P, et al (1996) Hippocampal volumes in Alzheimer's disease, Parkinson's disease with and without dementia, and in vascular dementia. Neurology 46:678–681. https://doi.org/10.1212/WNL.46.3.678
34. Lai MS-L, Sørensen MH, Lee K, et al (2024) 3D mapping of direct VTA-CA2 circuit with potential involvement in Parkinson's disease degeneration. Neurobiol Dis 202:106723.

https://doi.org/10.1016/j.nbd.2024.106723

35. Liu Q, Luo X, Liang Z, et al (2024) Coordination between circadian neural circuit and intracellular molecular clock ensures rhythmic activation of adult neural stem cells. Proceedings of the National Academy of Sciences 121:. https://doi.org/10.1073/pnas.2318030121
36. Liu X, Wang Q, Haydar TF, Bordey A (2005) Nonsynaptic GABA signaling in postnatal subventricular zone controls proliferation of GFAP-expressing progenitors. Nat Neurosci 8:1179–1187. https://doi.org/10.1038/nn1522
37. Loughlin SE, Foote SL, Bloom FE (1986) Efferent projections of nucleus locus coeruleus: Topographic organization of cells of origin demonstrated by three-dimensional reconstruction. Neuroscience 18:291–306. https://doi.org/10.1016/0306-4522(86)90155-7
38. Luskin MB (1998) Neuroblasts of the postnatal mammalian forebrain: their phenotype and fate. J Neurobiol 36:221–33
39. Martins-Macedo J, Araújo B, Anjo SI, et al (2024) Glial-restricted precursors stimulate endogenous cytogenesis and effectively recover emotional deficits in a model of cytogenesis ablation. Mol Psychiatry 29:2185–2198. https://doi.org/10.1038/s41380-024-02490-z
40. Marxreiter F, Regensburger M, Winkler J (2013) Adult neurogenesis in Parkinson's disease. Cellular and Molecular Life Sciences 70:459–473. https://doi.org/10.1007/s00018-012-1062-x
41. Mateus-Pinheiro A, Patrício P, Alves ND, et al (2021) Hippocampal cytogenesis abrogation impairs inter-regional communication between the hippocampus and prefrontal cortex and promotes the time-dependent manifestation of emotional and cognitive deficits. Mol Psychiatry 26:7154–7166. https://doi.org/10.1038/s41380-021-01287-8
42. McCall JG, Siuda ER, Bhatti DL, et al (2017) Locus coeruleus to basolateral amygdala noradrenergic projections promote anxiety-like behavior. Elife 6:. https://doi.org/10.7554/eLife.18247
43. McEwen BS, Nasca C, Gray JD (2016) Stress Effects on Neuronal Structure: Hippocampus, Amygdala, and Prefrontal Cortex. Neuropsychopharmacology 41:3–23. https://doi.org/10.1038/npp.2015.171
44. Medeiros D, Masini D, Plewnia C, et al (2024) Dopamine D2 receptor activation counteracts olfactory dysfunction and related cellular abnormalities in experimental parkinsonism. Heliyon 10:e35948. https://doi.org/10.1016/j.heliyon.2024.e35948
45. Mijatovic J, Airavaara M, Planken A, et al (2007) Constitutive Ret Activity in Knock-In Multiple Endocrine Neoplasia Type B Mice Induces Profound Elevation of Brain Dopamine Concentration via Enhanced Synthesis and Increases the Number of TH-Positive Cells in the Substantia Nigra. The Journal of Neuroscience 27:4799–4809. https://doi.org/10.1523/JNEUROSCI.5647-06.2007
46. Mizrak D, Levitin HM, Delgado AC, et al (2019) Single-Cell Analysis of Regional Differences in Adult V-SVZ Neural Stem Cell Lineages. Cell Rep 26:394–406.e5. https://doi.org/10.1016/j.celrep.2018.12.044
47. Mueller AD, Meerlo P, McGinty D, Mistlberger RE (2013) Sleep and Adult Neurogenesis: Implications for Cognition and Mood. pp 151–181

48. Nabizadeh F, Sodeifian F, Pirahesh K (2022) Olfactory dysfunction and striatal dopamine transporter binding in motor subtypes of Parkinson's disease. Neurological Sciences 43:4745–4752. https://doi.org/10.1007/s10072-022-06110-y
49. Ohira K (2020) Dopamine as a growth differentiation factor in the mammalian brain. Neural Regen Res 15:390. https://doi.org/10.4103/1673-5374.266052
50. O'Keeffe GC, Tyers P, Aarsland D, et al (2009) Dopamine-induced proliferation of adult neural precursor cells in the mammalian subventricular zone is mediated through EGF. Proceedings of the National Academy of Sciences 106:8754–8759. https://doi.org/10.1073/pnas.0803955106
51. Padulo C, Sestieri C, Punzi M, et al (2023) Atrophy of specific amygdala subfields in subjects converting to mild cognitive impairment. Alzheimer's & Dementia: Translational Research & Clinical Interventions 9:. https://doi.org/10.1002/trc2.12436
52. Patrício P, Mateus-Pinheiro A, Sousa N, Pinto L (2013) Re-cycling Paradigms: Cell Cycle Regulation in Adult Hippocampal Neurogenesis and Implications for Depression. Mol Neurobiol 48:84–96. https://doi.org/10.1007/s12035-013-8422-x
53. Paul A, Chaker Z, Doetsch F (2017) Hypothalamic regulation of regionally distinct adult neural stem cells and neurogenesis. Science (1979) 356:1383–1386. https://doi.org/10.1126/science.aal3839
54. Paxinos G, Watson C (2007) The Rat Brain in strereotaxic coordinates, 6th edn. Elsevier
55. Prange S, Klinger H, Laurencin C, et al (2022) Depression in Patients with Parkinson's Disease: Current Understanding of its Neurobiology and Implications for Treatment. Drugs Aging 39:417–439. https://doi.org/10.1007/s40266-022-00942-1
56. Privitera M, von Ziegler LM, Floriou-Servou A, et al (2024) Noradrenaline release from the locus coeruleus shapes stress-induced hippocampal gene expression. Elife 12:. https://doi.org/10.7554/eLife.88559.3
57. Qiu J, Takagi Y, Harada J, et al (2009) p27Kip1 Constrains Proliferation of Neural Progenitor Cells in Adult Brain Under Homeostatic and Ischemic Conditions. Stem Cells 27:920–927. https://doi.org/10.1002/stem.1
58. Regensburger M, Prots I, Winner B (2014) Adult Hippocampal Neurogenesis in Parkinson's Disease: Impact on Neuronal Survival and Plasticity. Neural Plast 2014:1–12. https://doi.org/10.1155/2014/454696
59. Ribeiro I, Silveira-Rosa T, Martins-Macedo J, et al (2025) Chronic stress and cytogenesis ablation disrupt hippocampal neuron connectivity, with fluoxetine restoring function with sex-specific effects. Neurobiol Stress 37:100743. https://doi.org/10.1016/j.ynstr.2025.100743
60. Seiriki K, Maeda S, Kojima L, et al (2025) Noradrenergic efferent subsystems that gate traumatic social learning
61. Seki K, Yoshida S, Jaiswal M (2018) Molecular mechanism of noradrenaline during the stress-induced major depressive disorder. Neural Regen Res 13:1159. https://doi.org/10.4103/1673-5374.235019

62. Sen S, Parishar P, Pundir AS, et al (2019) The expression of tyrosine hydroxylase and DARPP-32 in the house crow (< scp> *Corvus splendens* </scp>) brain. Journal of Comparative Neurology 527:1801–1836. https://doi.org/10.1002/cne.24649
63. Snyder JS, Grigereit L, Russo A, et al (2016) A Transgenic Rat for Specifically Inhibiting Adult Neurogenesis. eNeuro 3:ENEURO.0064-16.2016. https://doi.org/10.1523/ENEURO.0064-16.2016
64. Suzuki K, Okada K, Wakuda T, et al (2010) Destruction of Dopaminergic Neurons in the Midbrain by 6-Hydroxydopamine Decreases Hippocampal Cell Proliferation in Rats: Reversal by Fluoxetine. PLoS One 5:e9260. https://doi.org/10.1371/journal.pone.0009260
65. Takamura N, Nakagawa S, Masuda T, et al (2014) The effect of dopamine on adult hippocampal neurogenesis. Prog Neuropsychopharmacol Biol Psychiatry 50:116–124. https://doi.org/10.1016/j.pnpbp.2013.12.011
66. Teixeira FG, Carvalho MM, Panchalingam KM, et al (2017) Impact of the Secretome of Human Mesenchymal Stem Cells on Brain Structure and Animal Behavior in a Rat Model of Parkinson's Disease. Stem Cells Transl Med 6:634–646. https://doi.org/10.5966/sctm.2016-0071
67. Teixeira FG, Vilaça-Faria H, Domingues A V., et al (2020) Preclinical Comparison of Stem Cells Secretome and Levodopa Application in a 6-Hydroxydopamine Rat Model of Parkinson's Disease. Cells 9:315. https://doi.org/10.3390/cells9020315
68. Toda T, Parylak SL, Linker SB, Gage FH (2019) The role of adult hippocampal neurogenesis in brain health and disease. Mol Psychiatry 24:67–87. https://doi.org/10.1038/s41380-018-0036-2
69. Trivedi M (2004) Lesions of the ventral hippocampus, but not the dorsal hippocampus, impair conditioned fear expression and inhibitory avoidance on the elevated T-maze. Neurobiol Learn Mem 81:172–184. https://doi.org/10.1016/j.nlm.2004.02.005
70. Tsetsenis T, Broussard JI, Dani JA (2023) Dopaminergic regulation of hippocampal plasticity, learning, and memory. Front Behav Neurosci 16:. https://doi.org/10.3389/fnbeh.2022.1092420
71. Weihe E, Depboylu C, Schütz B, et al (2006) Three Types of Tyrosine Hydroxylase-Positive CNS Neurons Distinguished by Dopa Decarboxylase and VMAT2 Co-Expression. Cell Mol Neurobiol 26:657–676. https://doi.org/10.1007/s10571-006-9053-9
72. Wichmann T, Nelson A, Torres ERS, et al (2025) Leveraging animal models to understand non-motor symptoms of Parkinson's disease. Neurobiol Dis 208:106848. https://doi.org/10.1016/j.nbd.2025.106848
73. Wu K, Liu S (2024) Hippocampal dopamine as a key regulator for learning deficits in Parkinson's disease. Neural Regen Res 19:1193–1194. https://doi.org/10.4103/1673-5374.385860
74. Yamasaki M, Takeuchi T (2017) Locus Coeruleus and Dopamine-Dependent Memory Consolidation. Neural Plast 2017:1–15. https://doi.org/10.1155/2017/8602690
75. Yao Z, Fu Y, Wu J, et al (2020) Morphological changes in subregions of hippocampus and amygdala in major depressive disorder patients. Brain Imaging Behav 14:653–667. https://doi.org/10.1007/s11682-018-0003-1

76. Zhang L, Zhang P, Dong Q, et al (2024) Fine-grained features characterize hippocampal and amygdaloid change pattern in Parkinson's disease and discriminate cognitive-deficit subtype. CNS Neurosci Ther 30:. https://doi.org/10.1111/cns.14480
77. Zhao J, Jia H, Ma P, et al (2025) Multidimensional mechanisms of anxiety and depression in Parkinson's disease: Integrating neuroimaging, neurocircuits, and molecular pathways. Pharmacol Res 215:107717. https://doi.org/10.1016/j.phrs.2025.107717
78. Zheng F, Li C, Zhang D, et al (2019) Study on the sub-regions volume of hippocampus and amygdala in schizophrenia. Quant Imaging Med Surg 9:1025–1036. https://doi.org/10.21037/qims.2019.05.21

Figures

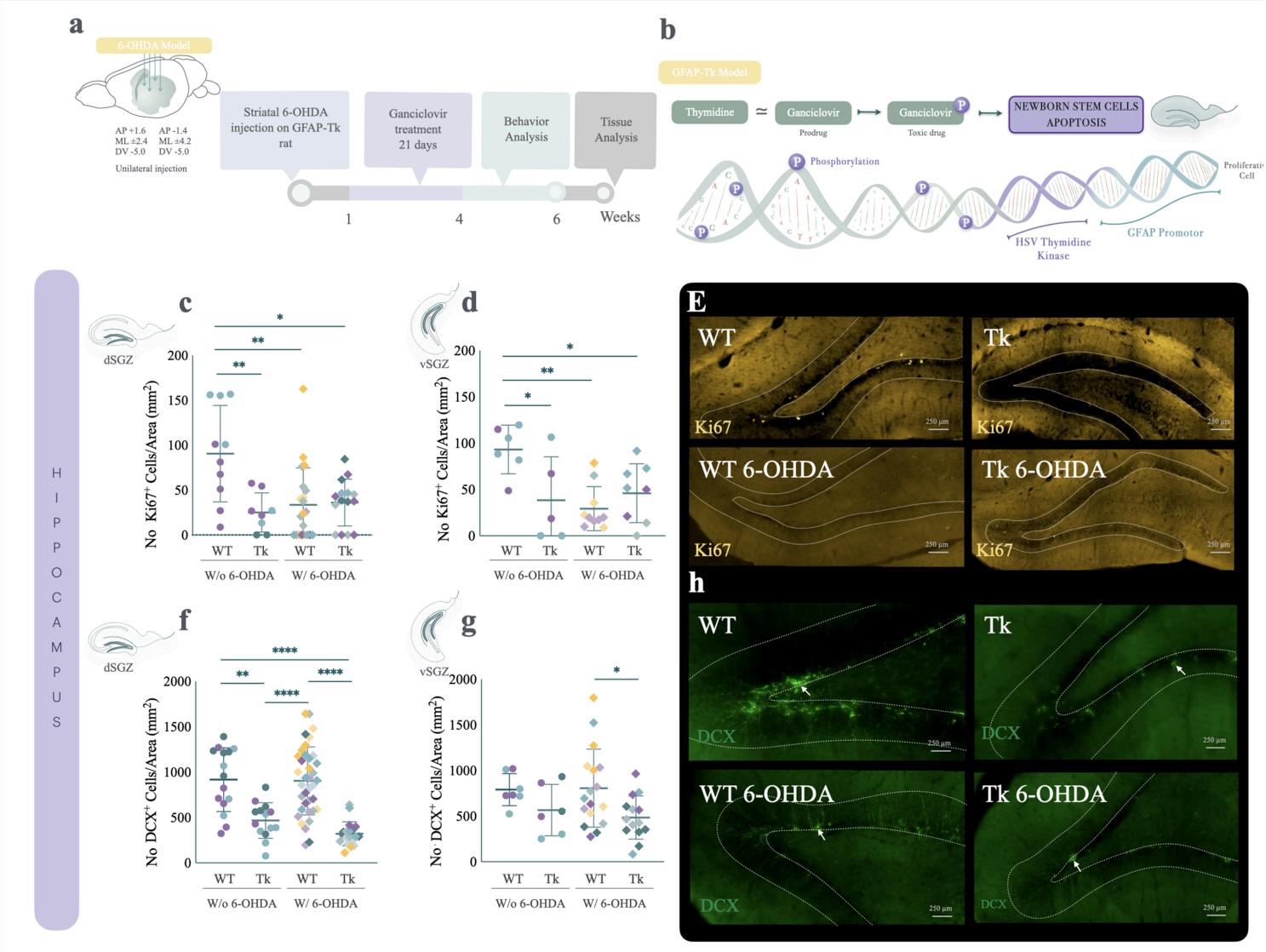


Figure 1

Hippocampal newborn cell survival in GFAP-Tk transgenic rats with 6-hydroxydopamine. a) A schematic representation of the experimental design. A unilateral surgery was performed on the GFAP-

Tk transgenic rats to administer 6-hydroxydopamine (6-OHDA) to induce degeneration of dopaminergic neurons. A few days later, b) ganciclovir treatment abrogated neurogenic events in the hippocampus. Motor performance was then evaluated, followed by histological analysis. c-e) Ganciclovir administration reduced the hippocampal proliferative and survival cell pool (Ki67+) in both the dorsal and ventral poles ($p<0.005$). f-h) Regarding neuroblast survival (DCX+), ganciclovir administration induced a significant decrease in the Tk groups compared to WT animals in the dorsal hippocampus ($p<0.005$). g-h) The ventral SGZ showed a specific reduction in neuroblasts in the Tk 6-OHDA group compared to 6-OHDA WT animals ($p=0.040$). Each colour in the graph represents the slices analysed by animal. Data are presented as mean ± SD, with statistical differences considered when $p<0.005$. *, $p<0.05$; **, $p< 0.0001$; ****, $p< 0.00001$. For Ki67 analysis, nº WT=2, nº Tk=3, nº WT 6-OHDA=6, nº Tk 6-OHDA=6. For DCX analysis, nº WT=3, nº Tk=3, nº WT 6-OHDA=7, nº Tk 6-OHDA=6. 1-2 dorsal hipocampal slices and 1-2 ventral hipocampal slices per animal. Both sides were analysed.

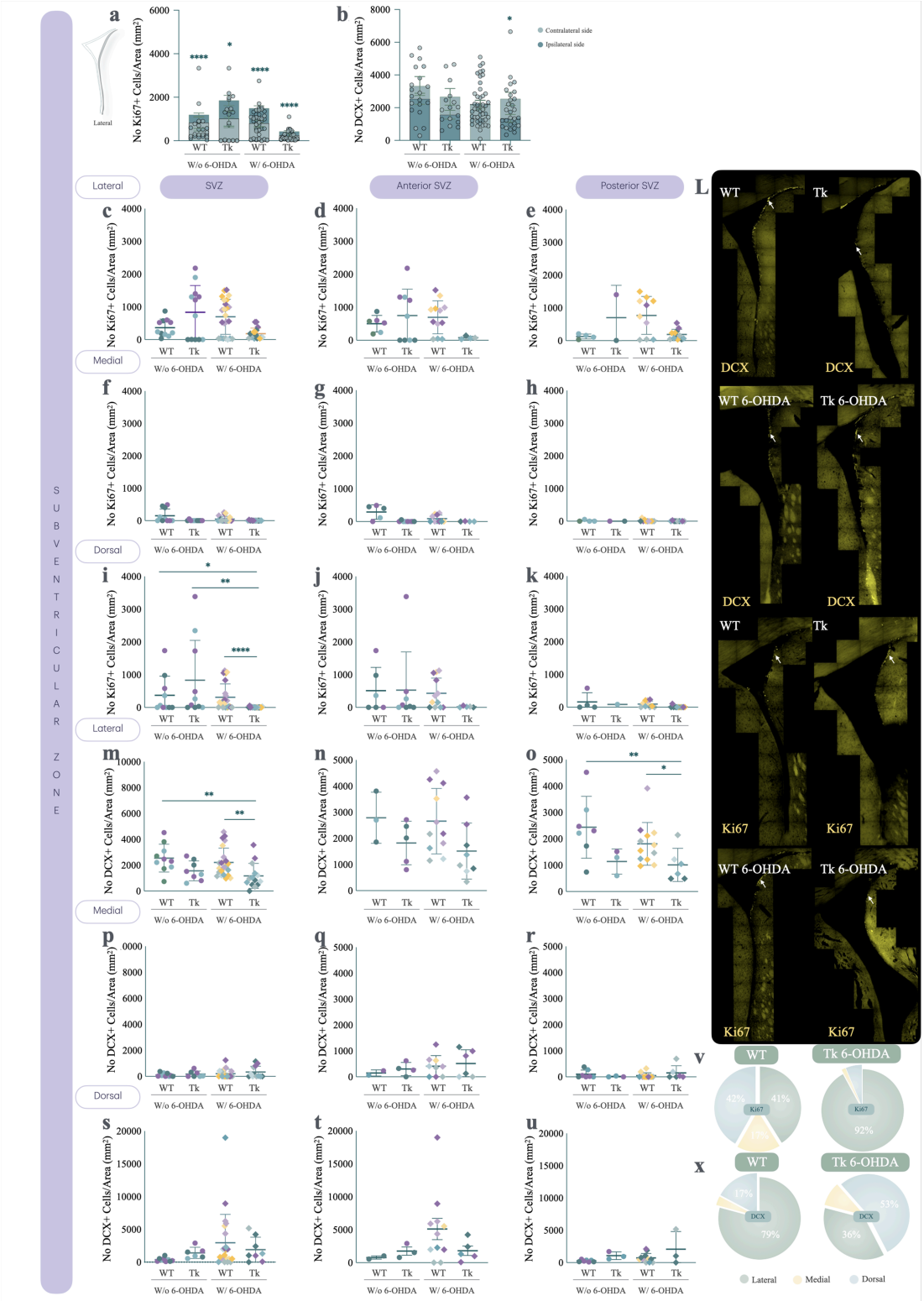


Figure 2

Survival of newborn cells in the subventricular zone of GFAP-Tk transgenic rats with 6-hydroxydopamine. a) The lesioned side exhibited a greater number of Ki67+ cells than the contralateral side ($p<0.001$). b) In contrast, the number of neuroblasts (DCX+) showed a significant difference between hemispheres in the Tk 6-OHDA group ($p=0.017$). c-x) The SVZ analysis was divided into subregions: lateral, medial, and dorsal. Additionally, each subregion was evaluated by anterior and

posterior coordinates. Thus, the first column of graphics shows the densities of Ki67 or DCX in the region, and the second and third columns demonstrate the densities in the anterior and posterior regions, respectively. d) In the anterior lateral region, Ki67+ cells were significantly reduced in the Tk 6-OHDA group compared to both WT and WT 6-OHDA animals ($p<0.001$). g) In the anterior medial region, all groups had fewer proliferating cells than WT animals ($p=0.005$). i) In the posterior dorsal region, Ki67+ cells exhibited lower densities in Tk 6-OHDA animals than in WT and WT 6-OHDA ($p=0.007$). m, o) Regarding neuroblast quantification (DCX+), in the posterior lateral zone, Tk 6-OHDA animals showed a reduced number of cells compared to WT and WT 6-OHDA ($p=0.024$). p-u) DCX densities did not vary significantly in the medial and dorsal regions. v-x) The pie charts show the qualitative distribution of the regions analysed in each group. v) Ki67+ cells were evenly distributed in WT animals, whereas in Tk 6-OHDA animals, they were mainly located in the lateral SVZ. x) In the case of DCX+ cells, they were mainly located in the lateral region in the WT group and, conversely, in the dorsal SVZ in the Tk 6-OHDA group. Each colour in the graph represents the slices analysed by animals. The data are presented as mean ± SD, with statistical differences considered when $p<0.005$. *, $p<0.05$; **, $p<0.001$; ****, $p<0.00001$. For Ki67 analysis, nº WT=2, nº Tk=3, nº WT 6-OHDA=7, nº Tk 6-OHDA=6. For DCX analysis, nº WT=3, nº Tk=3, nº WT 6-OHDA=7, nº Tk 6-OHDA=5. It was analysed 1-4 slices per animal. Both sides were analysed.

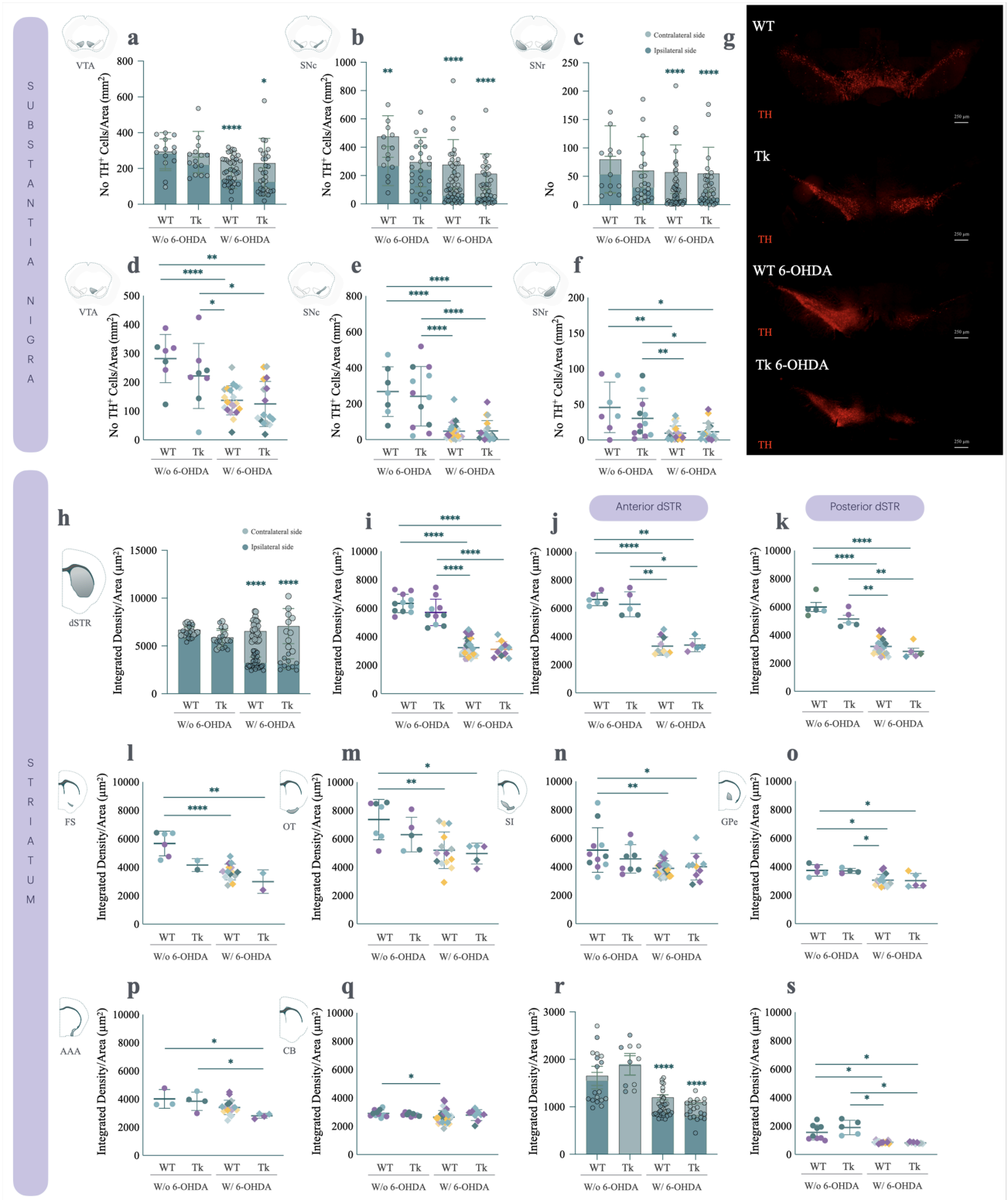


Figure 3

Fiber dopaminergic degeneration in the lesioned animals. a-c) Quantification of dopaminergic neurons (DAn) densities between hemispheres since the 6-hydroxydopamine (6-OHDA) was administered into the right side of the rats' brains. a) Thus, the injection of the neurotoxin contributed to a decreased in DAn in the VTA (Tk 6-OHDA: U=196, p=0.010), B) SNc (WT 6-OHDA: U=568, p<0.001; Tk 6-OHDA: U=310, p<0.001) and C) SNr (WT 6-OHDA: U=618, p<0.001; Tk 6-OHDA: U=299, p<0.001). Furthermore, we focus

the analysis on the ipsilateral side. d) The WT 6-OHDA and the Tk 6-OHDA animals presented a lower DAn density compared to the other non-lesioned animals in the VTA (p=0.001), e) SNc (p<0.001) and f) SNr (p=0.004), as it is notable in the representative fluorescence images. h) A reduction of dopaminergic fibers was observed in the ipsilateral side of the caudoputamen when comparing both hemispheres (WT 6-OHDA: p<0.001; Tk 6-OHDA: p<0.001). i) Considering the ipsilateral side, the caudaputamen showed a significant reduction between 6-OHDA and non-6-OHDA animals (p<0.001), which is evidenced both in the j) anterior (p<0.001) and k) posterior (p<0.001). Other regions analysed also exhibited differences between animals that received 6-OHDA and the groups which did not receive it L) FS: p=0.002; M) OT: p=0.003; N) SI: p=0.013; O) GPe: p=0.002; p) AAA: p=0.019; q) CB: p=0.044. r) Moreover, analyses of dopamine transporter (DAT) exhibited a significant reduction in the ipsilateral hemisphere of 6-OHDA-injected animals, WT 6-OHDA (p<0.001) and Tk 6-OHDA (p<0.001), compared to the other brain side. s) In the lesioned side, the overall decrease in DAT signal confirmed the DAn degeneration (*p<0.001*). The data is presented in mean ± SD, where the statistical differences were considered when p<0.005. *, p<0.05; **, p< 0.001; ****p< 0.00001. For SN analysis, nº WT=2, nº Tk=3, nº WT 6-OHDA=8, nº Tk 6-OHDA=6. For striatal analysis, nº WT=3, nº Tk=3, nº WT 6-OHDA=8, nº Tk 6-OHDA=6. It was analysed 1-4 slices per animal. Both sides were analysed.

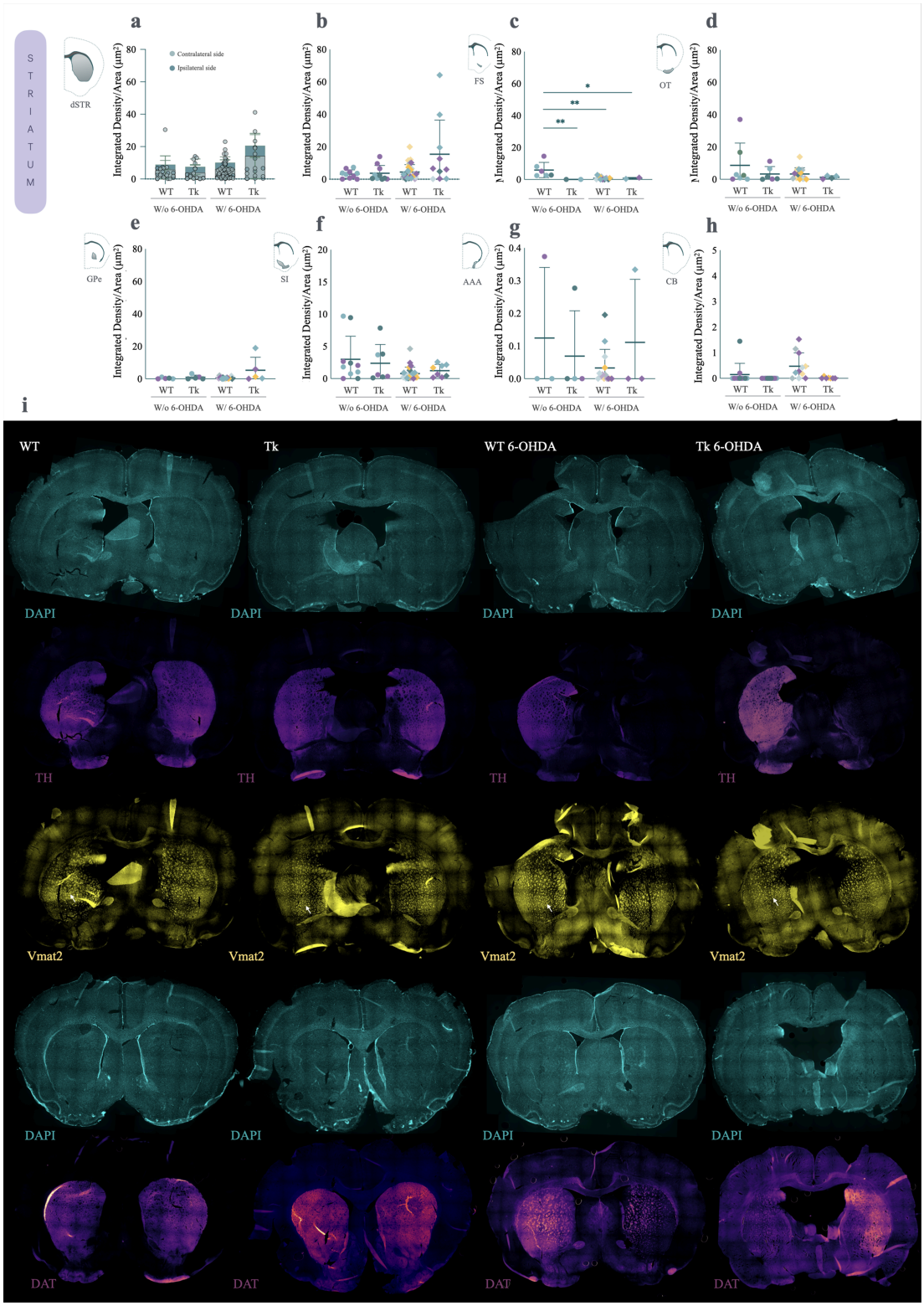


Figure 4

Vesicular monoamine transporter 2 (Vmat2) is present on dopaminergic neurons' fibers. a) The comparison between hemispheres did not demonstrate significant differences. a-g) Nevertheless, focusing on the ipsilateral side and on the regions where we detected significant statistical differences in the dopaminergic fibers, Vmat2 showed a significant decrease only in the fundus striatum region in the Tk, WT 6-OHDA, and Tk 6-OHDA groups (p=0.003). h) These data are followed by representative

fluorescent images of Tyrosine Hidroxylase (TH), Vmat2, and Dopamine Transporter (DAT) staining. Each color in the graph represents the slices analysed by animal.The data is presented as mean ± SD, with statistical differences considered when p<0.005. *, p<0.05; **, p<0.001. dSTR – dorsal striatum, FS – Fundus Striatum, OT – Olfactory Tubercle, GPe – Globus Pallidus external segment, SI – Substantia Inominata, AAA – Anterior Amygdalar Area, CB – Cingulate Bundle. For striatal analysis, nº WT=3, nº Tk=3, nº WT 6-OHDA=8, nº Tk 6-OHDA=6. It was analysed 1-4 slices per animal. Both sides were analysed.

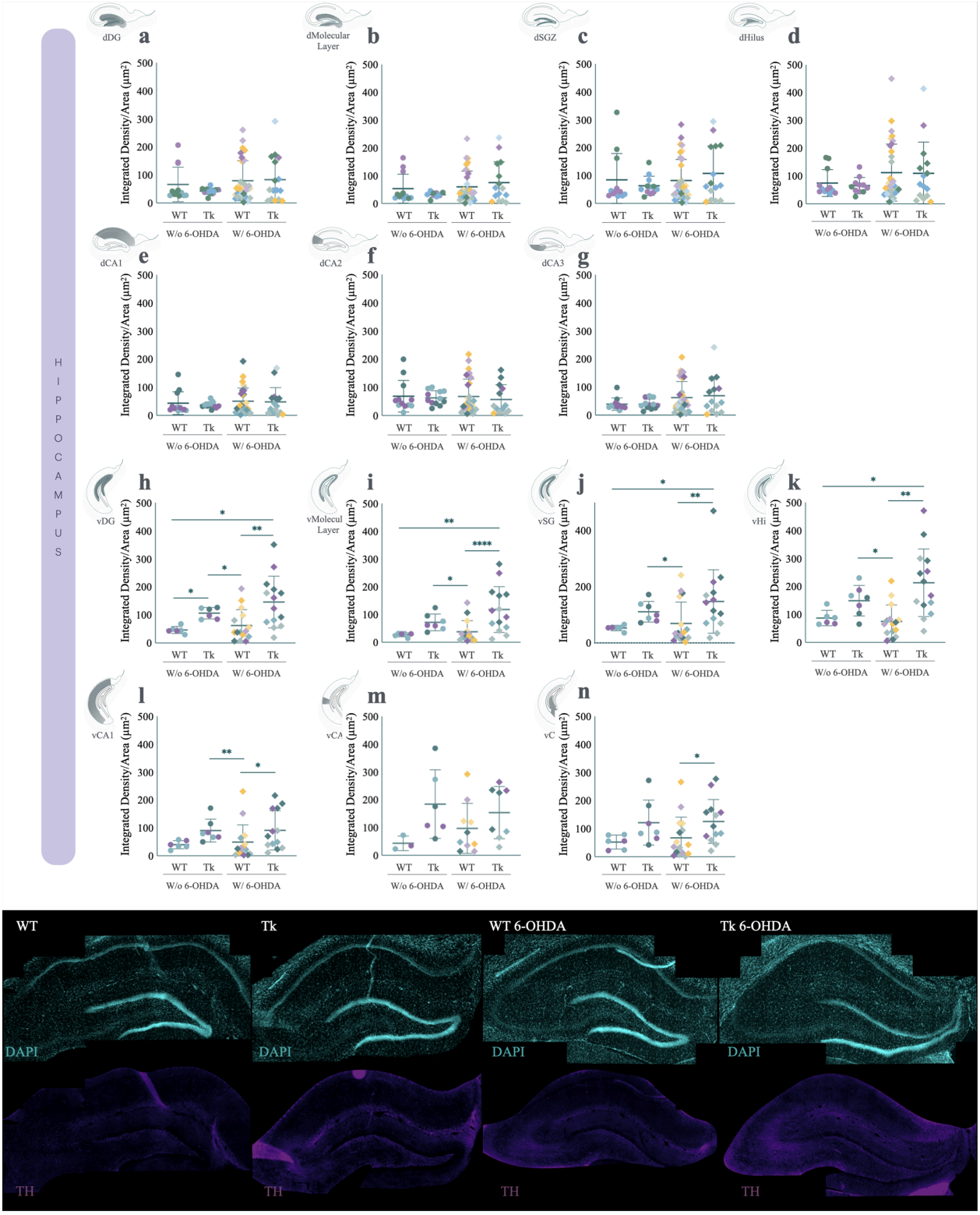


Figure 5

Tyrosine hydroxylase levels in the dorsal and ventral hippocampus. The hippocampus was analysed by sub-region: dentate gyrus (DG), molecular layer, subgranular zone (SGZ), hilus, and CA1-3. a-g) No significant differences were detected in the dorsal hippocampus sub-regions. In contrast, all sub-regions, except CA2 (m), showed a statistically significant increase in TH fluorescence intensity in Tks and Tks 6-OHDA animals compared with WT or/and WT 6-OHDA. h) ventral DG: p=0.003; i) ventral molecular: p=0.002; j) ventral SGZ: p=0.012; k) ventral hilus: p=0.001; l) ventral CA1: p=0.022; n) CA3: p=0.036. o) Representative fluorescent images of TH staining in the hippocampus. Each colour in the graph represents the slices analysed by animal. Data are presented as mean ± SD, with statistical differences considered when p<0.005. *, p<0.05; **, p<0.001; ****, p<0.00001. For hippocampal analysis, nº WT=3, nº Tk=3, nº WT 6-OHDA=8, nº Tk 6-OHDA=6. 1-2 dorsal hipocampal slices and 1-2 ventral hipocampal slices per animal. Both sides were analysed.

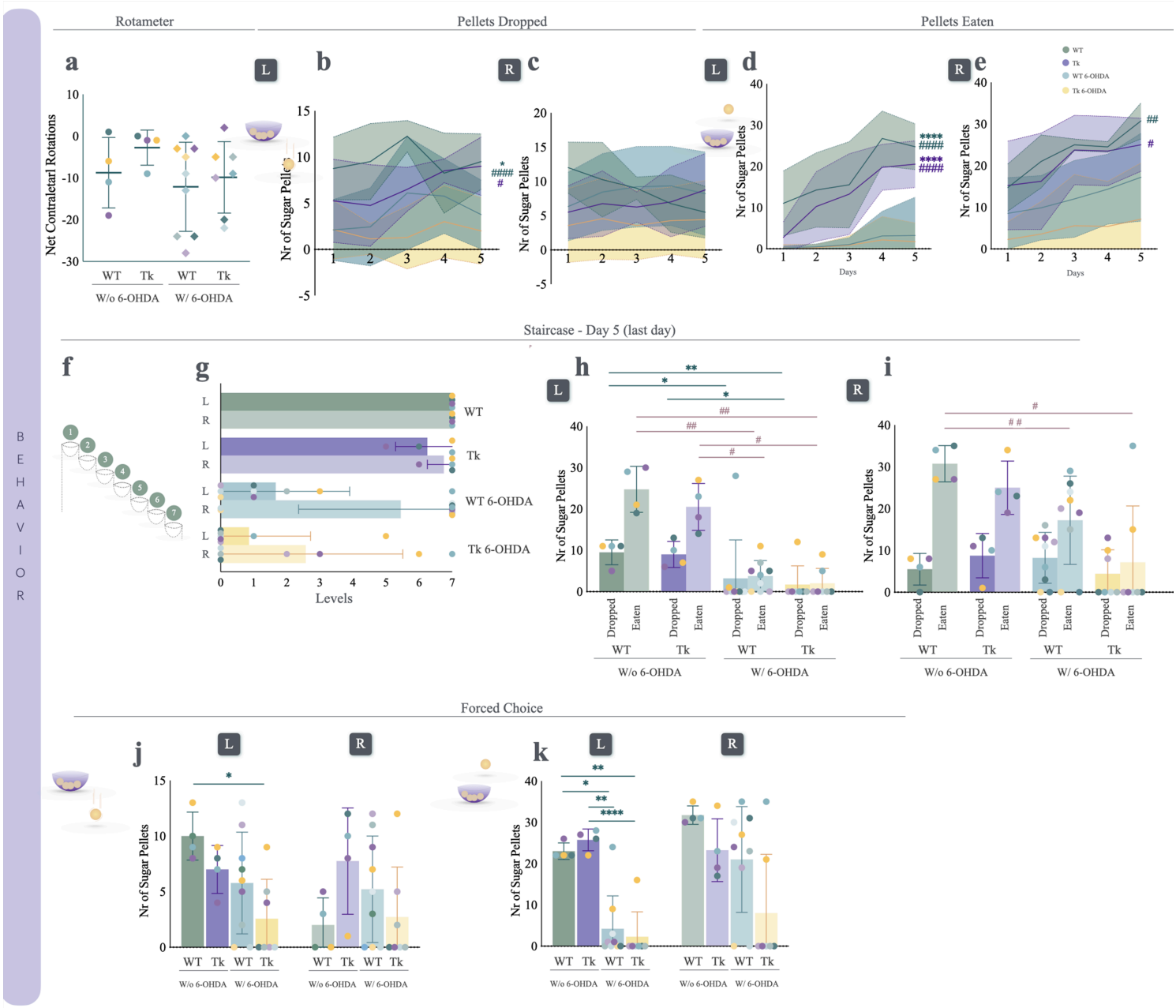


Figure 6

Motor behavior performance of animals with reduced hippocampal neurogenesis and/or dopaminergic neuron deficits. a) The apomorphine-induced rotational test did not show significant differences (p=0.387). b) However, the staircase test demonstrated motor deficits, as the ipsilateral side in the Tk animals dropped a higher number of pellets compared to the WT group, and the Tk 6-OHDA group showed similar statistical differences with the WT and WT 6-OHDA groups (WT vs Tk 6-OHDA, p<0.001; Tk vs Tk 6-OHDA, p=0.026) (Factor time: p=0.032; Interaction between factors: p=0.168; Factor treatment: p<0.001). C) On the other hand, the contralateral side did not show significant differences. d) Regarding the eaten pellets, Tk 6-OHDA animals reduced their success in retrieving and consuming pellets on the ipsilateral side (Factor time: p<0.001; Interaction between factors: p=0.019; Factor treatment: p<0.001). e) Contrary to other groups, Tk 6-OHDA also showed a reduction in the number of pellets they were able to reach and eat on the contralateral side (Factor time: p<0.001; Interaction between factors: p=0.422; Factor treatment: p<0.001). f, g) On the final day of the staircase test, lesioned animals had motor deficits when compared with the non-lesioned animals. h) The animal did not reach the sugar pellets with ease, as evidenced by the left members (dropped pellets: p=0.011), as with the i) right paws. However, a reduction in pellets eaten was observed in the 6-OHDA animals on the h) left and i) right sides (Left side: p=0.001; Right side: p=0.02), indicating their motor deficits. j) In the forced-choice condition, Tk 6-OHDA animals displayed severe impairments in consuming pellets on the ipsilateral side (dropped: p=0.037). k) Additionally, the same group showed difficulties in fine motor coordination, with fewer pellets eaten when the pellets were on the lesioned side (Eaten: p=0.001). k) Also, WT 6-OHDA animals could not retrieve sugar pellets on the ipsilateral side (p=0.001). j-k) On the other hand, the groups did not present differences on the right side on the last day of the staircase. The data are presented as mean ± SD, with statistical differences considered when p<0.05. *, p<0.05; **, p< 0.001; ***, p< 0.0001; ****, p< 0.00001. #, p<0.05; ##, p< 0.001. nº WT=4, nº Tk=4, nº WT 6-OHDA=8, nº Tk 6-OHDA=7. The symbol * denotes statistical differences from the WT 6-OHDA group, and the symbol # denotes statistical differences from the Tk 6-OHDA group.

Supplementary Files

This is a list of supplementary files associated with this preprint. Click to download.

- Table1.pdf
- AraujoBetal.SupplementaryFiguresLegend.docx
- SupplementaryFigure1.tiff
- floatimage1.jpeg
- SupplementaryFigure2.tiff